


Article

Performance of the Flexible and Rigid Lining under Earthquake Impact and Weakness of the New Austrian Tunneling Method (NATM) Principles, a Specific Case Study of the Bolu Tunnel

Ebu Bekir Aygar 

Fugro Sial Geosciences Consulting Engineering Ltd., Cankaya 06690, Ankara, Turkey; eaygar@gmail.com

Abstract: The Bolu tunnel is located between the Istanbul-Ankara Highway and its construction took approximately 13 years. Since the beginning of the tunnel excavation, serious deformations and stability problems have been encountered. The basis of the problems encountered during the tunnel excavation is the fact that the geological units through which the tunnel passes are very weak and fault lines cut the tunnel location. The fault lines pass through secondary faults in the seismically active North Anatolian Fault. At these fault crossings, deformations occurred continuously so that revisions had to be made in the support systems. The 12 November 1999 Düzce earthquake occurred on the Düzce fault and a surface rupture 40 km long was caused. The rupture terminated 1.5 km west of the tunnel; it did not reach the tunnel. Throughout the earthquake, instances of collapse occurred at the areas excavated on the fault line at the entrance of Elmalık and where the deformations exceeded 1.0 m; this section of the tunnel had to be abandoned. After these problems, a new improved design for tunnel excavation was developed. These new support systems, which are Bernold lining and bench pilot tunnel systems, contain allowance for rigid lining that is the opposite of the new Austrian tunneling method (NATM) principles. Within the scope of this study, the causes of the collapse in the tunnel are investigated and the effect of the Düzce earthquake on the tunnel is discussed. Also, the applicability of the NATM in tunnels excavated on weak zones is also discussed.



Citation: Aygar, E.B. Performance of the Flexible and Rigid Lining under Earthquake Impact and Weakness of the New Austrian Tunneling Method (NATM) Principles, a Specific Case Study of the Bolu Tunnel.

Sustainability **2023**, *15*, 15544.
<https://doi.org/10.3390/su152115544>

Academic Editors: Deyu Qian
and Zhiyi Zhang

Received: 16 August 2023
Revised: 25 September 2023
Accepted: 12 October 2023
Published: 1 November 2023



Copyright: © 2023 by the author. Licensee MDPI, Basel, Switzerland. This article is an open access article distributed under the terms and conditions of the Creative Commons Attribution (CC BY) license (<https://creativecommons.org/licenses/by/4.0/>).

Keywords: Bolu tunnel; 12 November 1999 Düzce earthquake; tunnel collapse; NATM

1. Introduction

Underground structures are widely known as less susceptible structures to earthquakes than those on the surface. Moreover, for deep tunnels, such as those passing through rocks, the impact of earthquakes is almost non-existent. However, when they approach the surface and/or pass through soil units rather than rocks, a huge increase in the effect of earthquakes on tunnels and underground structures is expected. There are several studies that have been conducted on the effect of earthquakes on tunnels [1–20]. The Düzce earthquake, which occurred on 12 November 1999 with a moment magnitude of 7.2, killed approximately 1000 people and injured 5000 people, and the event caused heavy structural damage. Also, many researchers have studied the Düzce earthquake [21–29].

The 1999 Düzce earthquake occurred three months after the 1999 İzmit earthquake, both along the North Anatolian fault (NAF) in northwest Turkey. The 1999 Düzce earthquake (Mw: 7.2) originated from the Düzce fault within the NAF zone. The Düzce fault is an active right-lateral strike-slip fault, delimiting the Düzce basin from the south. The earthquake produced an approximately 40 km-long right-lateral strike-slip surface rupture, running in the east–west direction between Golyaka and the Bolu tunnel [24,30]. The rupture geometry and slip distribution were well documented in Duman et al. 2005 [30]. This work proposes that the earthquake nucleated on the middle section of the Düzce fault, and the rupturing bilaterally propagated towards the west and east. The rupture extended along the southern margin of the Düzce basin between Golyaka to the west and the Asarsuyu

valley to the east. The width of the rupture zone varies from a few meters to 0.8 km. The width of the deformation zone increases at both stepovers and bends. Maximum and average right-lateral displacement were measured as 5.3 and 3.5 m, respectively, to the east; the Kaynasli section of the rupture diagonally crossed the E-80 highway and the Trans-European Motorways (TEM) highway viaducts. A 3.8 km-long easternmost portion of the rupture followed the Asarsuyu valley and terminated 1.5 km west of the northern entrance of the Bolu tunnel. Right-lateral strike-slip displacements of about 1.5 m were observed along the TEM highway viaducts, representing openings on the structures [30]. Along the Asarsuyu section, from the west to the eastern tip, the dextral slip decreased from 0.55 m to 3–5 cm [30]. There was no surface rupture observed in the tunnel area [31]. Peak ground accelerations (PGA) were recorded as 0.8 g at Bolu Station, which is 30 km away from the tunnel [2].

The highway tunnels are in a first-degree seismic zone in the North Anatolian fault zone and were drastically affected by the Düzce earthquake on 12 November 1999. The epicenter of the Düzce earthquake was approximately 20 km from the northern Asarsuyu portals of the tunnels [32]. During the 12 November 1999 Düzce earthquake, a collapse occurred at the side of the Elmalık entrance where the tunnel's inner (final) concrete lining had not been installed yet, leading to the abandonment of the Elmalık entrance (facing the direction of Ankara). Figure 1 shows the tunnel in the aftermath of the Düzce earthquake. No damage occurred at the entrance sections of the tunnel where the inner lining had been installed. At the Asarsuyu entrance of the tunnel (facing towards Istanbul city), no collapse problems were observed in the sections where the inner lining had been installed, except an occurrence of the fissures in the shotcrete and partial defects/deformations in the sections without the inner (final) concrete lining (Figure 2).

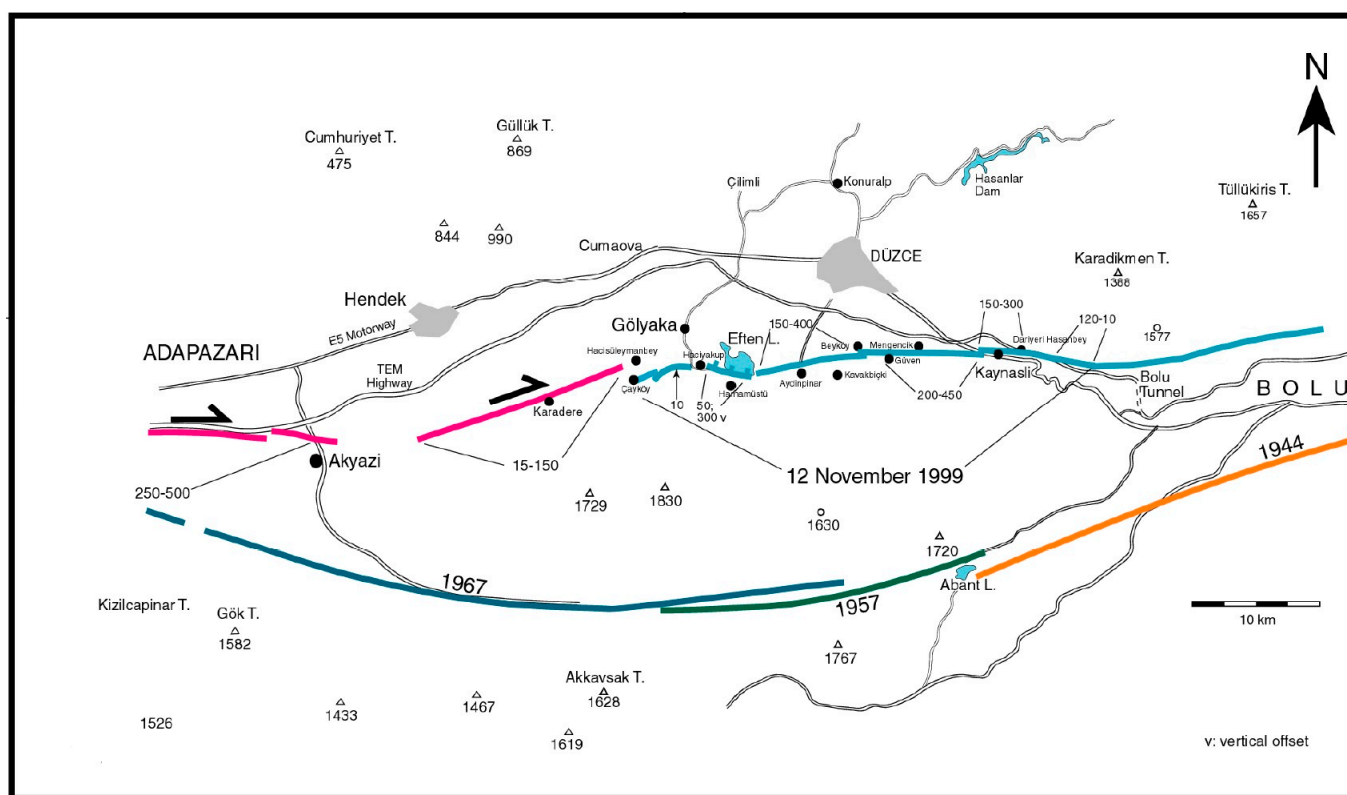


Figure 1. The surface rupture after the 12 November 1999 Düzce earthquake and active faults around Bolu and the slip distribution and extents of the rupture zones of the 1944 (orange), 1957 (green), 1967 (blue), 1999 İzmit (red), and Düzce (light blue) earthquakes [31].

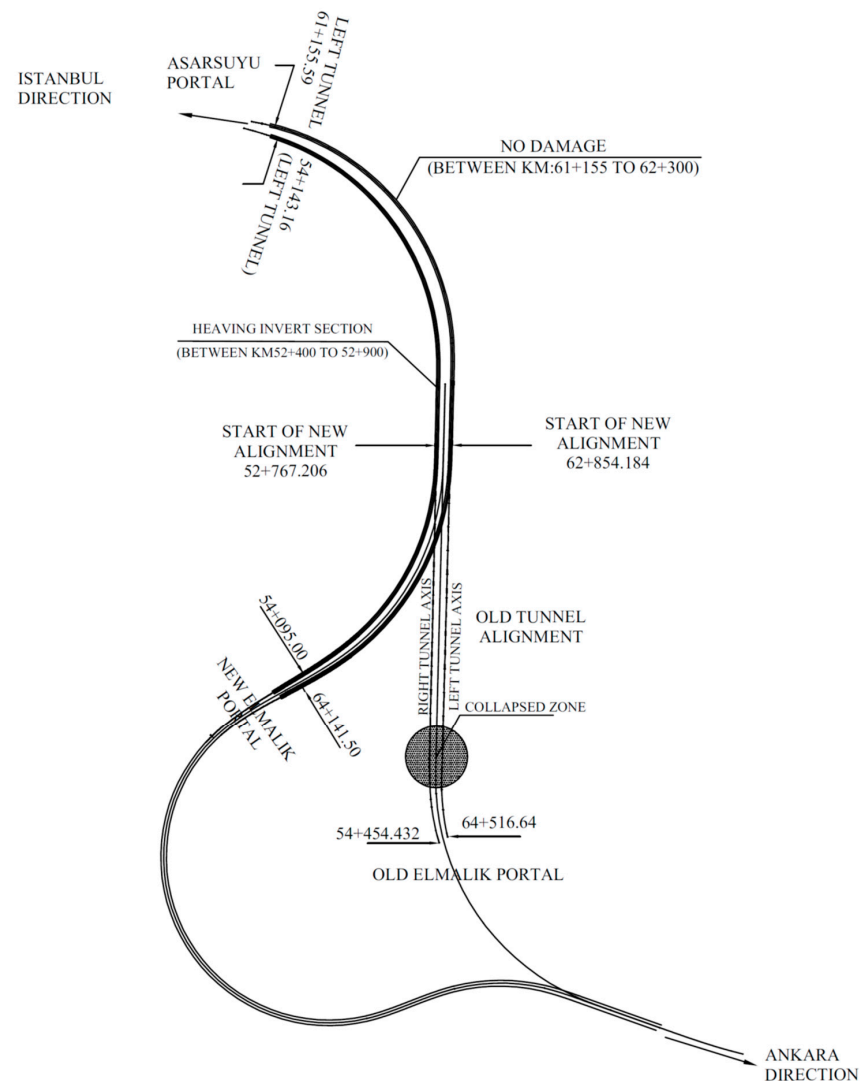


Figure 2. Distribution of damage after the 12 November 1999 Düzce earthquake.

Although it is commonly stated that underground structures are less affected by earthquakes than surface structures [3,33–35], serious problems were encountered in the fault zones and shallow overburden during the earthquake [36,37]. Special support systems were required in active fault zone transitions. For example, in the T9 tunnel opened within the scope of the Ankara–Sivas High-Speed Railway Project, seismic joints were used during the active fault crossing to minimize the impact of an earthquake [38].

In this study, the investigation methodology implicated is given as:

- geological and geotechnical conditions;
- seismicity of the Bolu tunnel and the Düzce earthquake;
- support systems in the Bolu tunnels;
- geotechnical instrumentation;
- analysis of support system with analytical solutions;
- the impact of the Düzce earthquake on the Bolu tunnel;
 - investigation of the Elmalık side;
 - investigation of the Asarsuyu side;
 - evaluation of geotechnical measurements;
 - inner lining design after the Düzce earthquake;
- Conclusions.

The main cause of the collapse is investigated, being either the earthquake or an insufficient support system. In addition, the NATM principles and failed principle under these circumstances is discussed in this paper. Furthermore, the tunnel support design philosophy is also discussed.

2. Bolu Tunnel

The Bolu tunnel is located within the Trans European Motorways (TEM) crossing between Düzce and Bolu cities on the Istanbul–Ankara Highway (Figure 3). Tunnel excavation had started in 1993 and it took 13 years to be completed, in 2006. Eventually, the tunnel was opened to traffic in 2007.

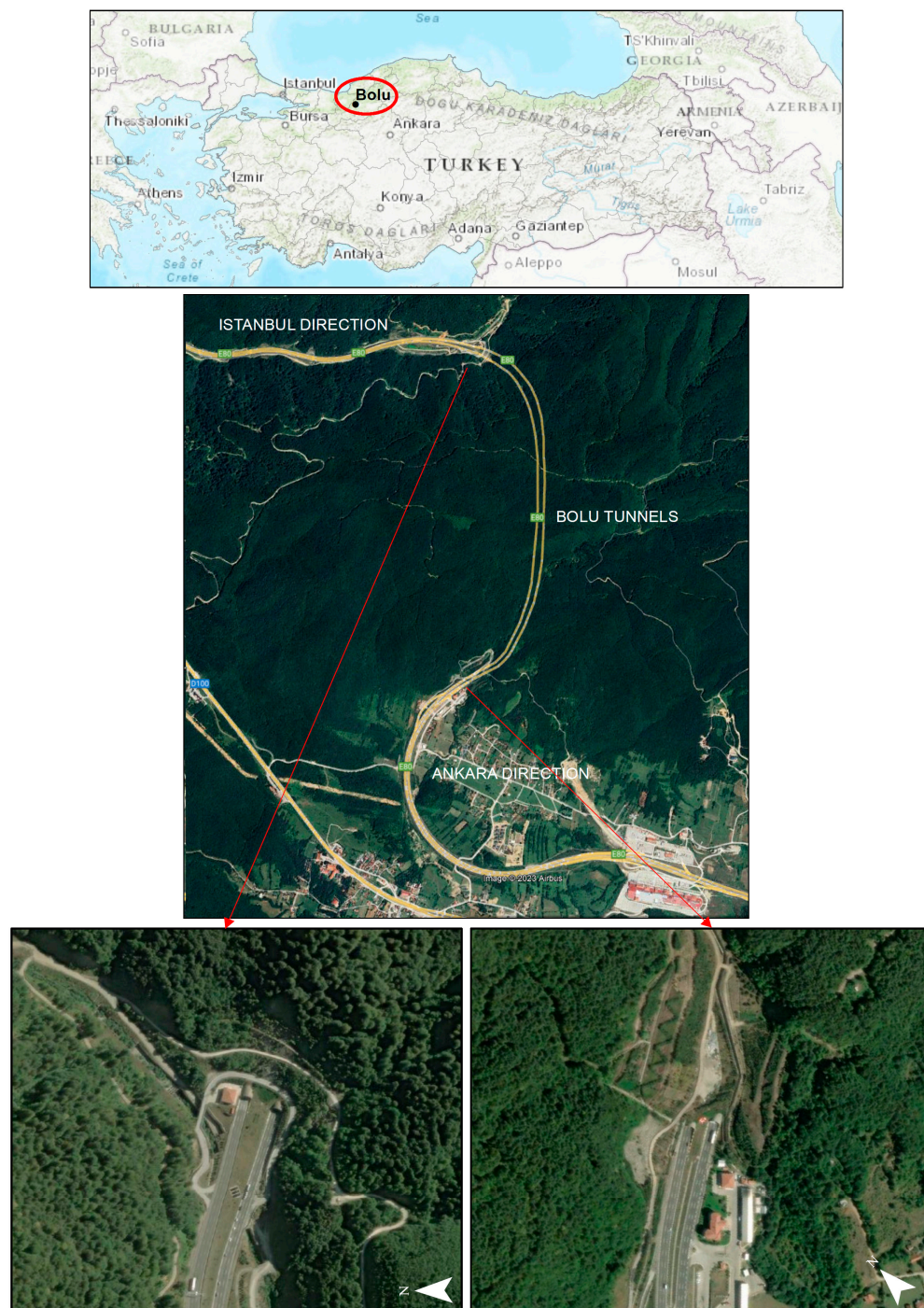


Figure 3. Bolu tunnel location map and portal sections.

After the examination of tunnel properties, an average of 50–60 m of toe was left between each tunnel in order to avoid possible adverse interaction between the tunnels. The overburden thickness above the tunnels was up to 250 m. Regarding the tunnel type sections and support system features, tunnel excavation areas were a minimum of 133 m² and a maximum of 260 m². Tunnel excavation diameters ranged between 13.0 m and 18.2 m, depending on the support system features. At the end of the processes, the final height and width of the tunnel were 8.60 m and 14.0 m, respectively.

Geological and Geotechnical Conditions

The geological conditions were determined based on the geological and geotechnical investigations throughout the project design phase of the Bolu tunnels, wherein the geological conditions encountered were different from the prediction. The main reason for this difference was the inadequacy of the field studies conducted during the aforementioned project design phase. The tunnels were excavated through faulted rock sequences which had been subjected to extensive tectonism. The main fault systems in this region were classified as first degree active seismic faults. The lithology of the units generally consists of semi-angular blocks of hard material appearing in clayey environments. The distribution of clayey environments varies for different geotechnical units, so that there are large regions of fault clay in the weakest ground conditions. The volumetric ratio of clayey environments ranges between 30% and 100%. Some parts representing the weakest conditions consist of formation sequences in which there is scarcely any hard material content, but merely fault clay. Along the tunnel route, weak formations were excavated with a thickness reaching up to 50 m. The youngest tectonic structures in the region are naturally the vertical or almost vertical dips, depending on impacts of the North Anatolian fault system. At some regions of the tunnel, it was observed that there were potentially sliding large blocks on slickensided and polished surfaces dipping towards the tunnel face. This situation was frequently encountered along the tunnel route. The mentioned negative factors caused excessive and unpredicted sudden deformations inside the tunnels [39]. On the other hand, the geology encountered at the entrance of Elmalık includes the flysch series consisting of claystone, siltstone, and limestone, mixed and highly tectonized, with rigid, generally polished–slickensided surfaces and highly plastic fault clay materials in and around the fault zone. At the entrance of Asarsuyu, generally metasediment series and crushed zones formed by these series were observed. This geological unit continued through the Bakacak fault transition. In the study of Lettis and Barka (2000) [31] and the report prepared accordingly, it states that the Bakacak fault is approximately 10 to 15 km long and crosses the Bolu tunnel within a 200 m wide fault zone. The orientation of the fault in this part is approximately towards the east–west direction. This fault intersects the tunnel route with an almost right angle between km: 62 + 800–km: 63 + 000 (left tunnel). These faults have north-directed subduction angles illustrated on cross-sections, and cross the tunnel with a fault clay material of 75 m width in the left tunnel and 91.5 m width in the right tunnel (Figure 4). This fault clay material is composed of metasediment units (metasiltstone, metalimestone, quartz–limestone, crystallized limestone, low to medium plastic, firm and stiff sandy silty fault clay matrix, slickensided and polished surfaces, and dry to moist water conditions), quartz rocks, amphibolite, and a metacrystalline layer (weathered crystalline rock). The mentioned fault zone material is found at the junction of the Asarsuyu–Elmalık geological formations. On the contrary, the fault zone material encountered at the tunnel elevation is a series composed of two different characterized units: the first unit is dark brown, highly plastic, and with a rigid–highly rigid polished surface, whereas the second unit is reddish brown, medium plastic, and with a very rigid–hard polished surface. The units encountered in the Bolu tunnels can be divided into four main groups. These are the metacrystalline layer (the Yedigöller formation), the metasediment series (the İkizoluk formation), the flysch series (the Findıcak formation), and the clayey fault zones [40]. The oldest unit in the tunnel route is the Yedigöller formation, which is formed by metamorphic rocks at the Asarsuyu entrance. The İkizoluk formation comprising the Devonian aged

metamorphic sequence overlays this formation with a tectonic contact. Above these, there are intrusive granite with tectonic contact and various sedimentary rocks from Upper Cretaceous to Upper Eocene [41]. A lithological section containing granodiorite altered by amphiboles is observed at the entrance of Asarsuyu. There are altered granodiorites and amphiboles mixed with sandstone, quartzites, and marbles. The connection between the crystalline basement and the overlaying sediment cover is formed by overlapping fault layers dipping at an unpredictably low angle. The whole section is highly fractured and transversely covered by fault layers having clayey—fault clay—regions. Moreover, at the Elmalık entrance, the limestone basement shows itself as interspersed sections among the materials dominated by clayey layers with sandstones and limestone blocks. The whole series has clayey faults and fault fillings. The geological and geotechnical profiles are presented in Figure 5.

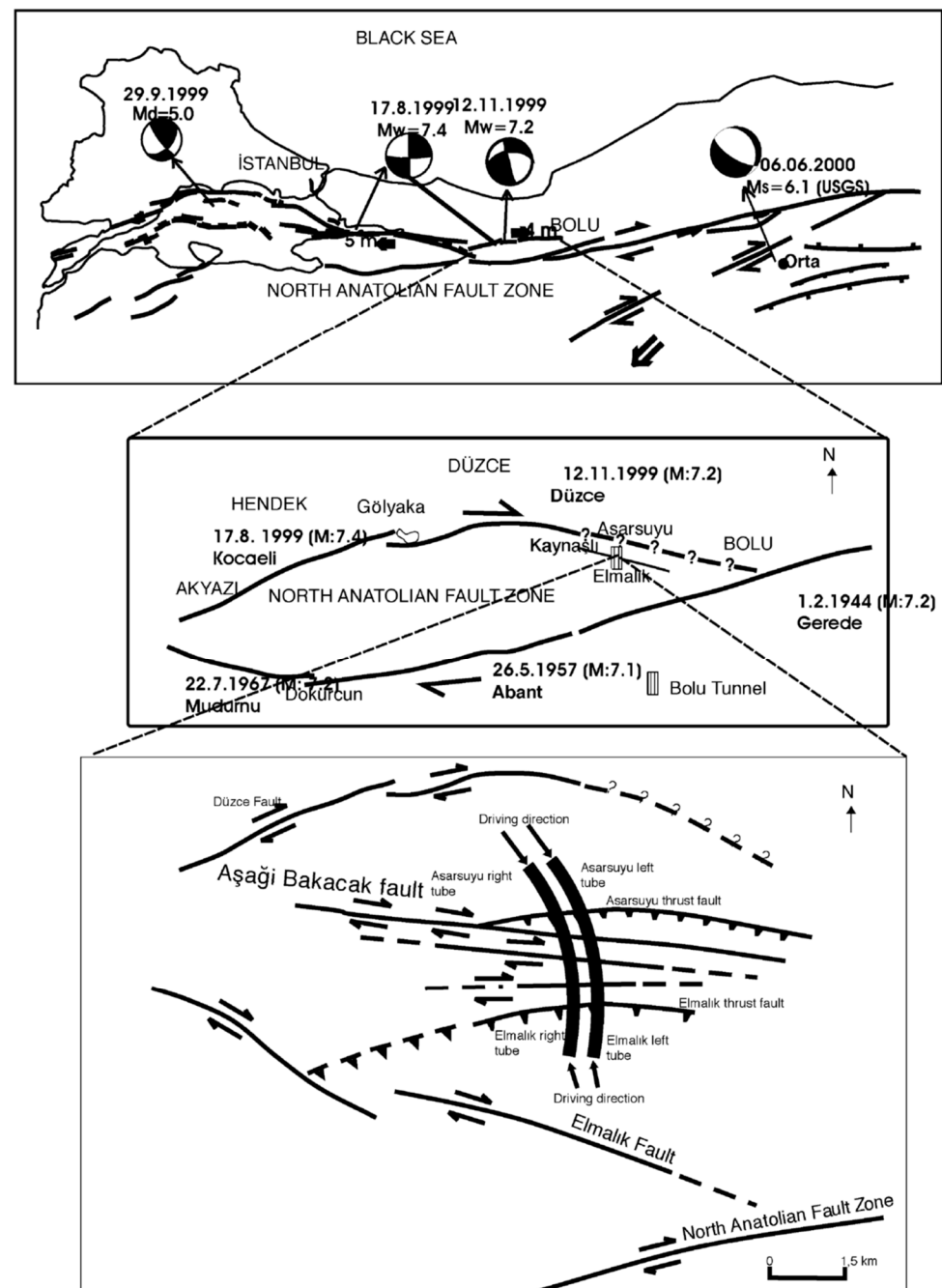


Figure 4. The Bakacak fault cross-section in the tunnel [40].

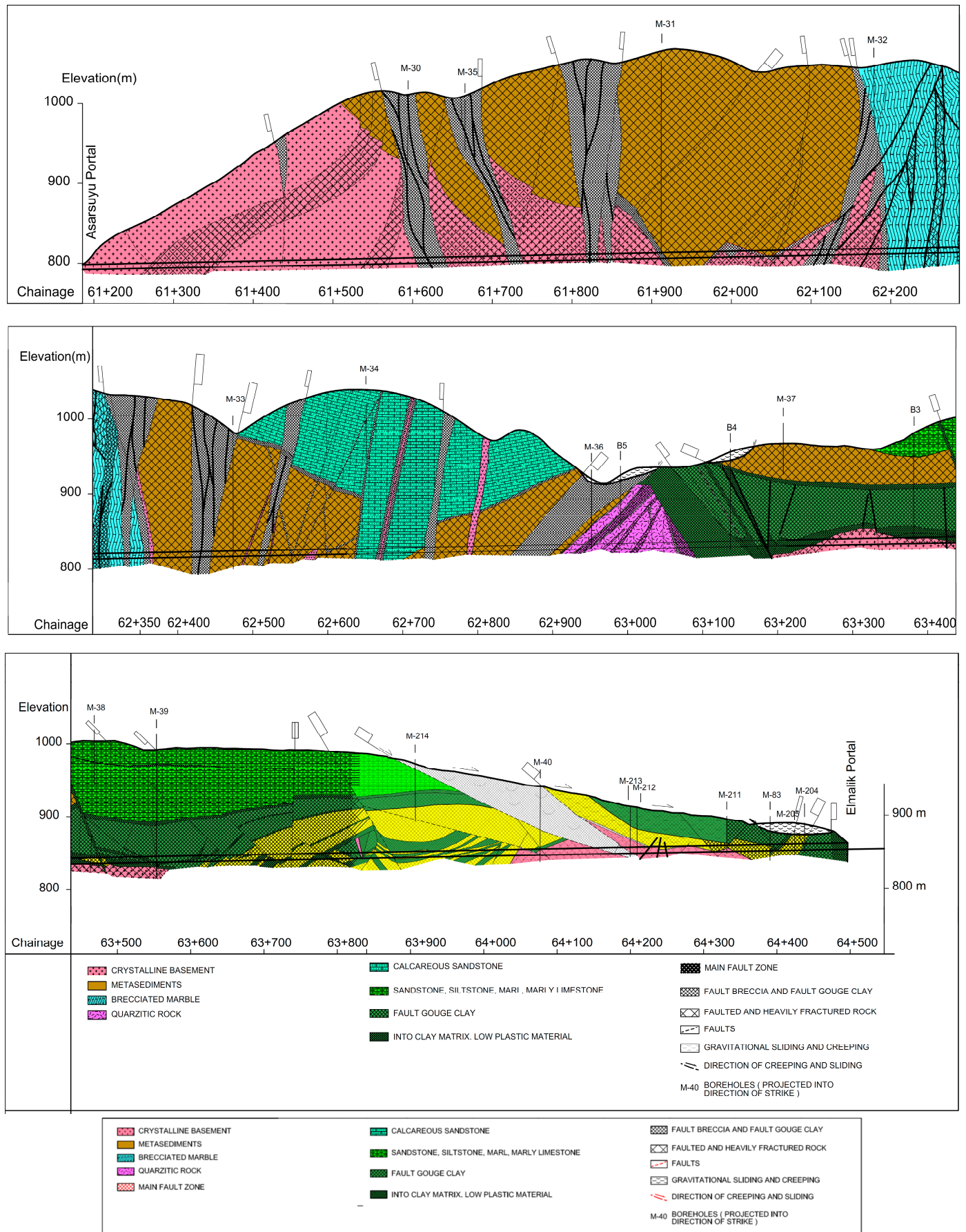


Figure 5. Bolu tunnel geological and geotechnical profiles [42].

In 1998 and 1999, a detailed characterization of the ground ahead of the tunnel faces was implemented via a pilot tunnel test program. The identified geotechnical units and their mechanical properties are described in Table 1 [43].

Table 1. Measured strength and stiffness parameters [43].

Unit	Peak		Residual		G_0/σ'_v ⁷
	ϕ' ⁶	c' ⁶ (kPa)	ϕ' ⁶	c' ⁶ (kPa)	
High PI ⁵ flysch clay	15°–17°	100	9°–12°	50	500 ¹
Blocky flysch clay	20°–25°	100	13°–17°	50	650 ¹
Area 3 FG ³ clay	13°–16°	100	9°–12°	50	700 ¹
AS/EL FG ³ clay	18°–24°	100	6°–12°	50	NA ⁴
Metasediments	25°–30°	50	20°–25°	25	825 ¹
Crushed MCB	20°–25°	50	15°–20°	25	950 ¹
Sound MCB ²	55°	1500	NA ⁴	NA ⁴	High

¹: From high-quality pressure meter tests. ²: Metacrystalline basement rock. ³: Fault gouge. ⁴: Not available. ⁵: Plasticity index. ⁶: ϕ' , c' = effective stress friction angle and cohesion, respectively. ⁷: G_0/σ'_v = ratio of max shear modulus to initial vertical effective stress.

3. Seismicity of the Bolu Tunnel

The 12 November 1999 Düzce earthquake gave rise to a surface rupture of approximately 40 km length, starting from south of Golyaka in the west and extending to the east of Kaynaşlı. It stands for a two-sided fracture whose location of outer center relevant to surface rupture developed along the east–west direction and emerged from the outer center of the earthquake. The earthquake ruptured the western end of the Karadere fault (KFS), which also had broken in the 1999 East Marmara earthquake in the west, along 9 km. The fracture observed in the field continued along the Düzce fault after the Eften Lake structure. The largest vertical offset of the surface rupture along the EGC formed as 3 m (Figure 6) [44].

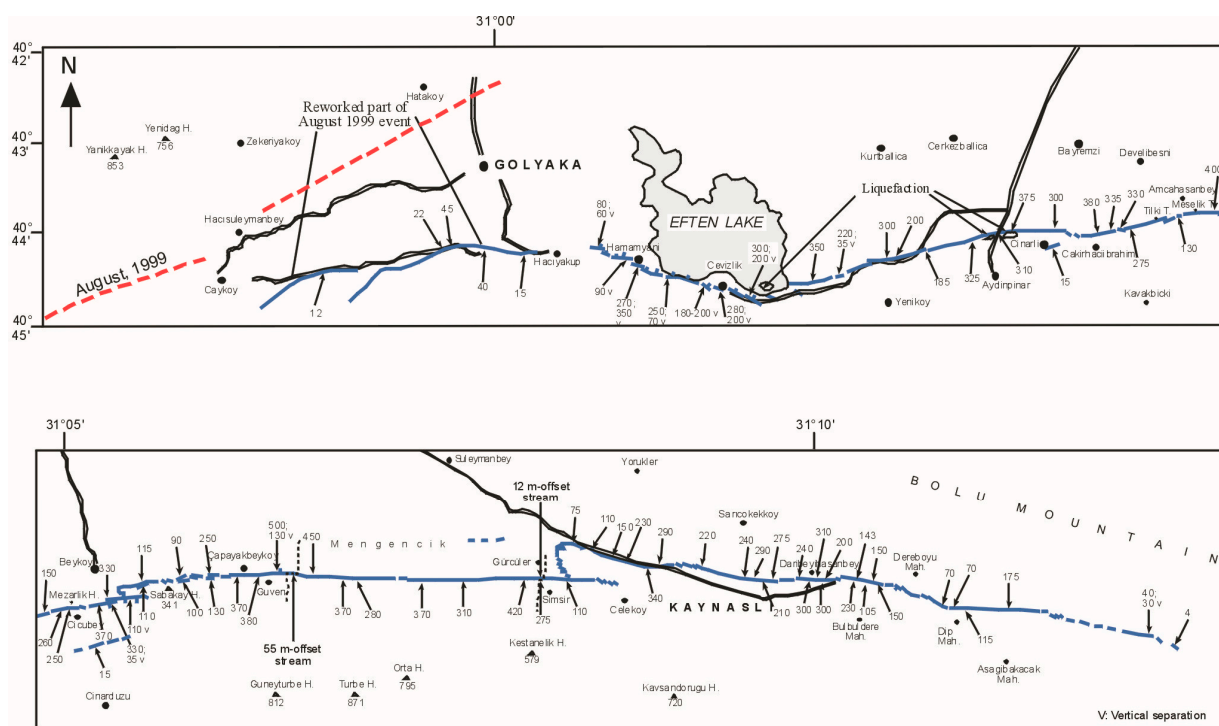


Figure 6. Surface rupture geometry of the 12 November 1999 Düzce earthquake [31].

The Gumusova–Gerde Motorway Project is located between the two active branches of the North Anatolian Fault System (Figure 7). The route passes through several faults such as the Düzce, Elmalık, Bakacak, Zekidagi, and Dipsizgol faults [31].

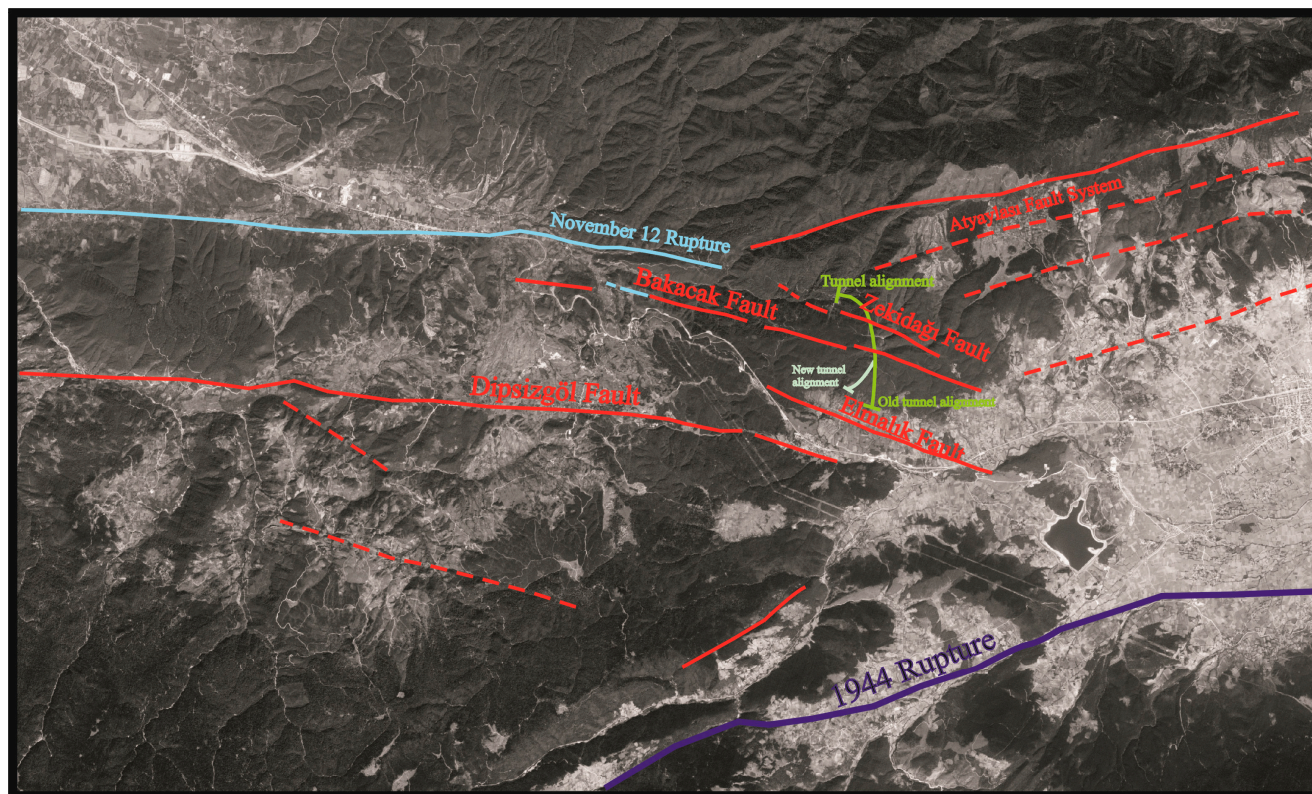


Figure 7. Local main faults (red), 1999 Düzce earthquake rupture (light blue), and 1944 Bolu Gerde rupture zone (dark blue) intersection [31].

The Bakacak and Zekidagi faults, which intercept the Bolu tunnel, are active faults. The Bakacak fault is 10–15 km length and has severe effects on the tunnel. The Zekidagi fault is 6–8 km long and affects the tunnel in a relatively minor aspect [31]. The interaction of the Bakacak fault with the Bolu tunnel is presented in Figure 4.

The Bakacak fault caused a small movement in the western part of the fault during the Düzce earthquake of 12 November 1999. However, in the evaluations made [31], it was found that the Bakacak fault was tensed and turned into an approximate future rupture. For this reason, special support systems were applied in the Bolu tunnel at the Bakacak fault transition [45,46]. Two different scenarios were produced for the Bakacak fault, as below [31].

1. The Bakacak fault may be reactivated in the future with high-intensity earthquakes in the Bolu section, regarding the North Anatolian fault line or the Düzce fault. The Bakacak fault extends as a connection fault between these two faults. During the 1999 Düzce earthquake, movements occurred in the western part of the Bakacak fault. The Düzce fault and the Bolu part of the North Anatolian fault were activated in the earthquakes of 1944 and 1999, respectively. In these sections, it is expected that there will be huge earthquakes in the next 50 to 100 years;
2. In addition, the Bakacak fault may play a part in moderate earthquakes. Depending on the fault length and rupture area, the Bakacak fault may produce earthquakes having magnitudes of 6.25 to 6.5. Average depth of the surface rupture is expected to be approximately between 30 and 50 cm after these potential earthquakes. It is known that there are strong geomorphic conditions associated with a specific section of the Bakacak fault lying between the main section of the Bakacak fault towards the Bolu tunnel.

Depending on the fault length and the rupture area of the fault, the Zekidagi fault is able to generate earthquakes having a magnitude around 6 to 6.25 on the Richter scale. The occurrence of surface rupture may also cause displacements ranging from approximately 15 to 35 cm. Starting from the Elmalık section of the tunnel route, the tunnels cut the Elmalık fault into two main sections. The Elmalık fault has a length of 10 to 15 km. Similar to the Bakacak fault, some scenarios are also expected for the Elmalık fault [31], as follows:

1. The Elmalık fault can be segregated under the effect of high-magnitude earthquakes on the North Anatolian fault line and the Düzce fault. The Elmalık fault is located between the Düzce fault and the main North Anatolian fault. The 1944 Bolu–Gerede earthquake induced ruptures on the Elmalık fault, and, contrary to that, the Düzce earthquake did not rupture the Elmalık fault;
2. The Elmalık fault will be activated in a moderate earthquake. The fault will produce an earthquake of 6.25 and 6.5 magnitude, depending on the length and the rupture area, and will cause displacement between 30 and 50 cm on average, but may, potentially, reach up to 1 m at maximum.

4. Support Systems Applied in the Bolu Tunnel and Stability Problems in the Elmalık Entrance Collapsed Zone

Different types of support system combinations were implemented during the tunnel excavation due to encountering very weak ground conditions in the Bolu tunnel. During the preliminary phase, the Bolu tunnel was designed based on the NATM principles. The NATM philosophy is based on the principle of maximizing the capacity of the ground to sustain its own weight by precisely and rationally balancing the pressures that affect the surrounding rock and support [46]. The basic principle of the NATM is to utilize thin and flexible lining, whereas the excavation section is divided into stages, which are top heading, bench, and invert.

In the first design phase, weak ground condition is accommodated with design consistent with C2 support class according to NATM class [47] sections, with suggested 25 cm shotcrete (Figure 8). However, upon encountering stability problems and extreme deformations in the tunnel, the support systems were revised as C3, C3-M, and intermediate lining (Figures 9 and 10). Intermediate lining, which is called Bernold lining, contains lining between the outer and inner linings. After completing the outer lining (shotcrete, bolts, and steel rib), the intermediate lining (Bernold lining) was installed with a lining thickness of 60 cm (C40 concrete class) to prevent extra loads and deformations before the inner lining was installed (Figures 9 and 10) [45,46]. In the large fault zones, the bench pilot tunnels method was applied to prevent deformation (Figures 11 and 12). The bench pilot tunnels method involves two pilot tunnels in the bench section, which have diameters of 5 m constructed before the top heading excavations. After completing the bench pilot tunnel with reinforced C30 concrete, the top heading excavation was started. As shown in Figures 11 and 12, the bench pilot tunnel method is a very rigid support system.

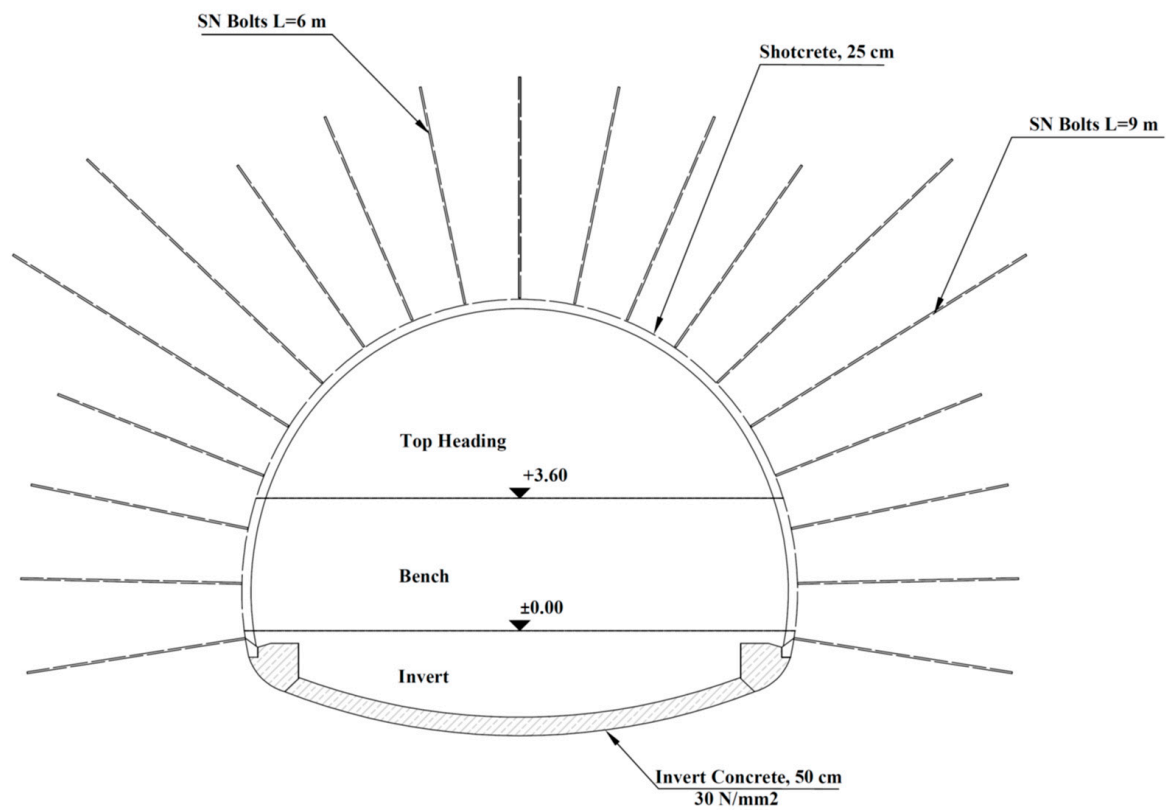


Figure 8. C2 Support system details proposed in the first design phase [48].

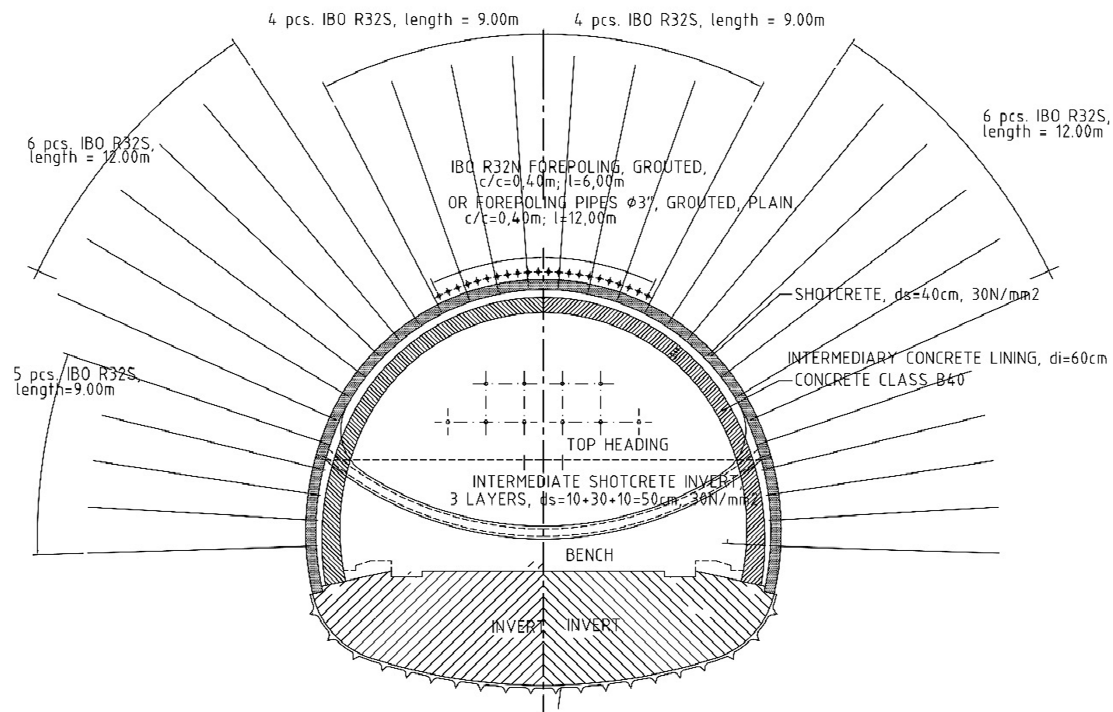


Figure 9. Intermediate lining (Bernold Lining) method implemented at minor fault zone and fly-schoide series [49].

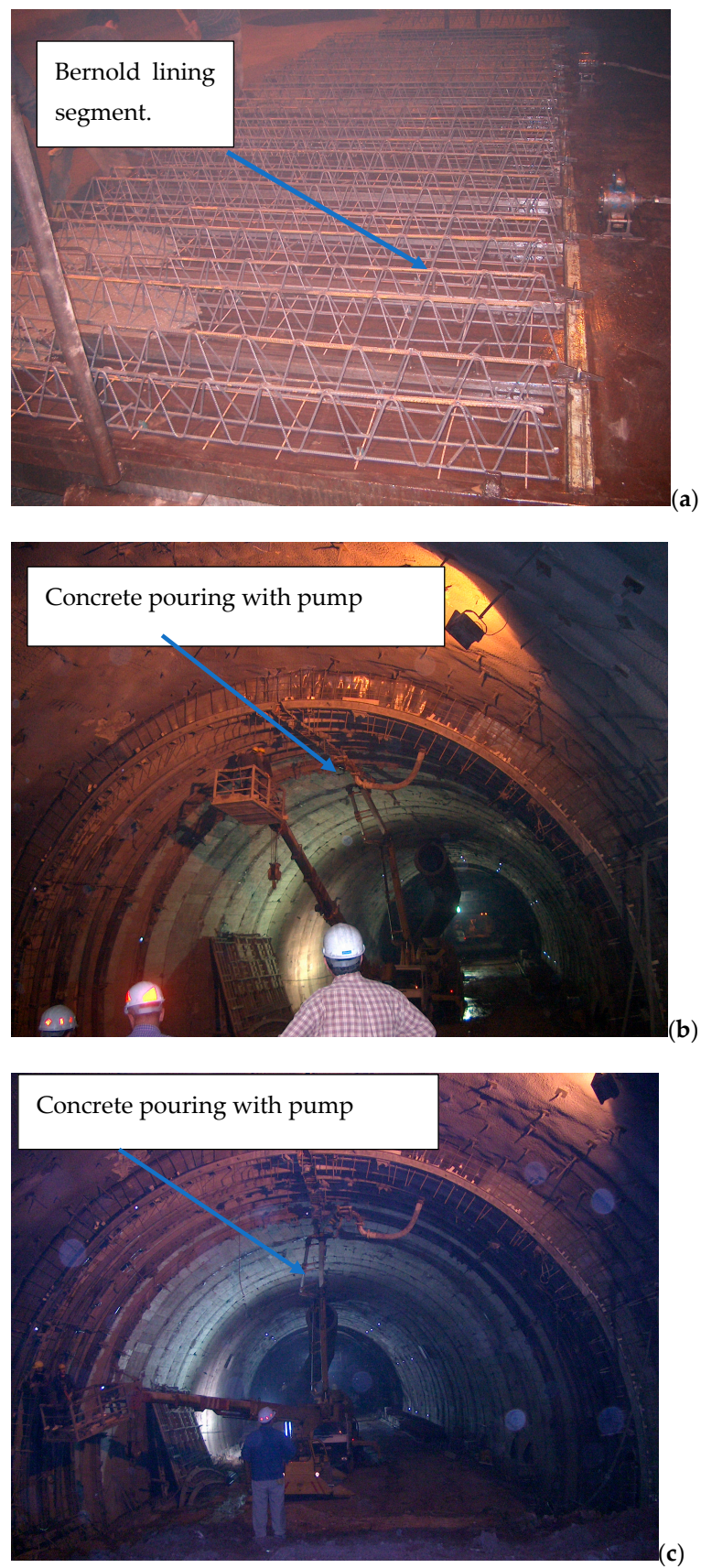


Figure 10. Intermediate lining (Bernold) method applications: (a) Bernold lining support; and (b,c) pouring the concrete to the Bernold lining back.

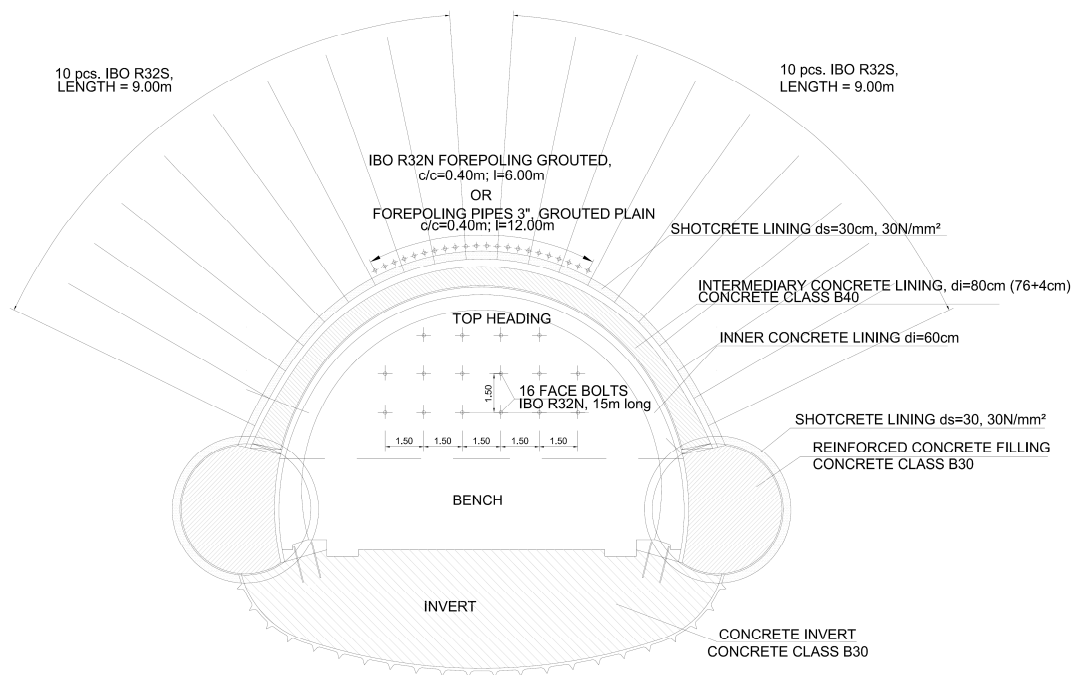


Figure 11. Bench pilot tunnel method implemented at major fault zones [50].



Figure 12. Bench pilot tunnel method applications.

Both methods (the Bernold lining and the bench pilot tunnels) are the opposite of the NATM principles. Both these two lining methods are aiming to mitigate deformations from occurring during the tunnel excavation. Moreover, no collapse or failure occurred in the fault zone or the flyschoid series during the earthquake where these methods were applied. The tunnel support principle should be a rigid system to prevent deformations under the conditions of weak ground and a large cross-section. Otherwise, the displacements could not be stabilized. In the Bolu tunnel applications, it has been seen that the NATM principles failed; therefore, all assumptions and design philosophy were changed. This situation has proved to be a very important point regarding NATM tunnelling and needs to be revised.

Geotechnical Instrumentations in the Tunnel

Deformation measurement points were placed every 10 m along the tunnel route. At these points, the soil behavior was examined by measuring the deformations regularly. Extensometer, pressure cell, and strain gauges were placed within the fault zones and flysch series. The geotechnical measurement points in the tunnel are shown in Figure 13.

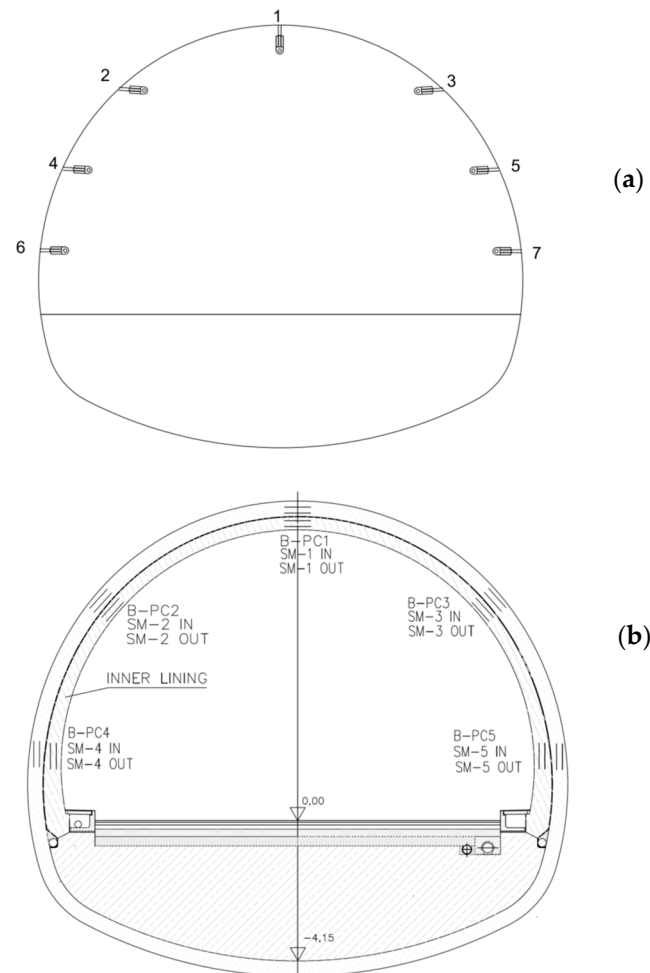


Figure 13. Geotechnical measurements points: (a) deformation points; and (b) strain gauge and pressure cell measurement points.

The deformation measurements taken in the Elmalık left tunnel fault zone are presented in Figure 14. At the fault zones and flysch series, deformations exceeding 1.0 m were observed prior to implementation of the intermediate lining and the bench pilot tunnel method (Figure 11). The displacement graphs of the tunnel are presented in Figure 14. The greatest displacement measured is on the left shoulder at readings 4 (+). At this point, the main reason for the greatest displacement is the effect of the right tunnel on the left tunnel. Because the readings used belong to the left tunnel, point 4 is the closest point to the right tunnel. This situation caused severe stability problems, thus, local rescreening and reinforcement were performed (Figure 14). After deformations had reached up to 100 cm, this part of the tunnel completely collapsed as a result of the force implemented by the Düzce earthquake.

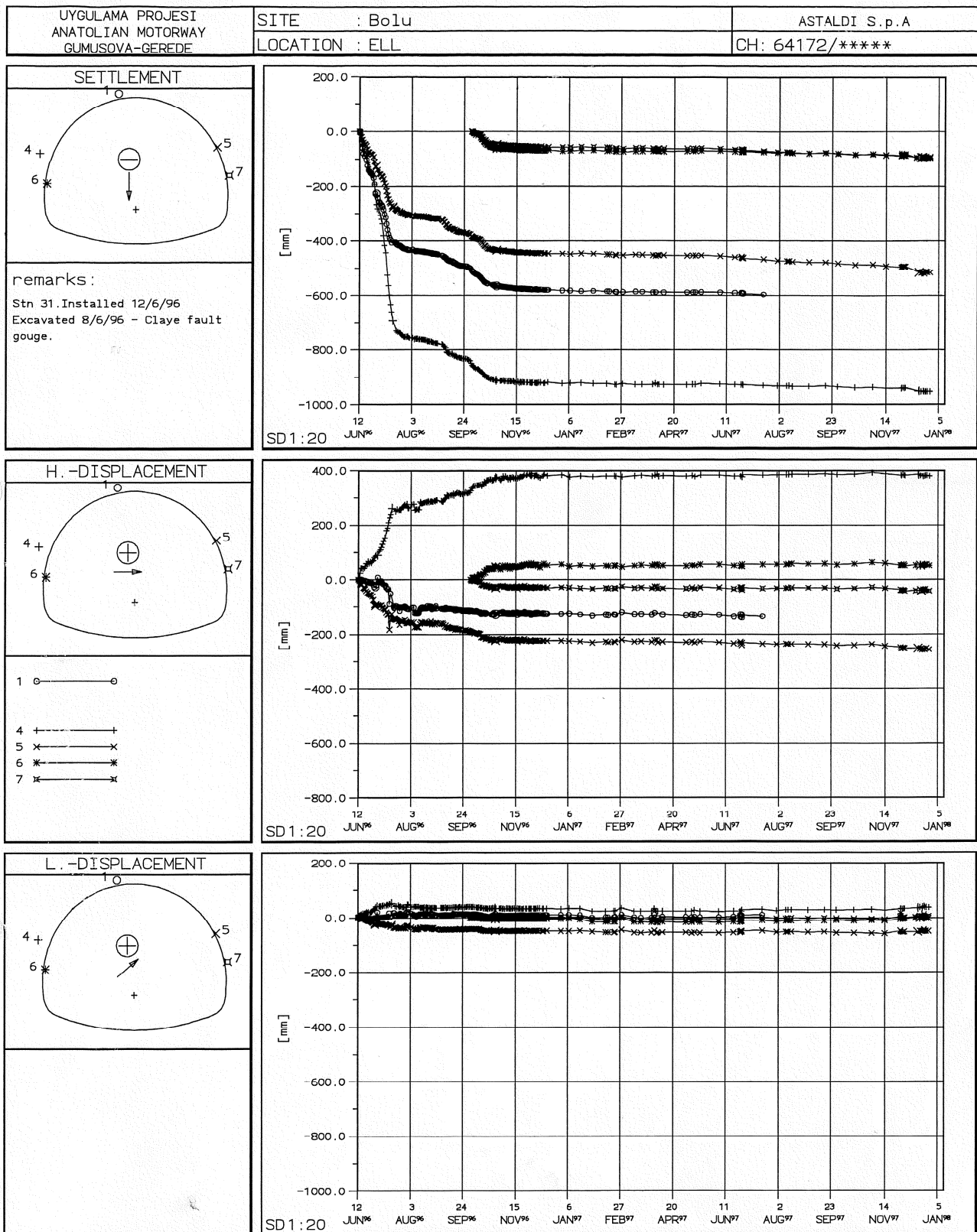
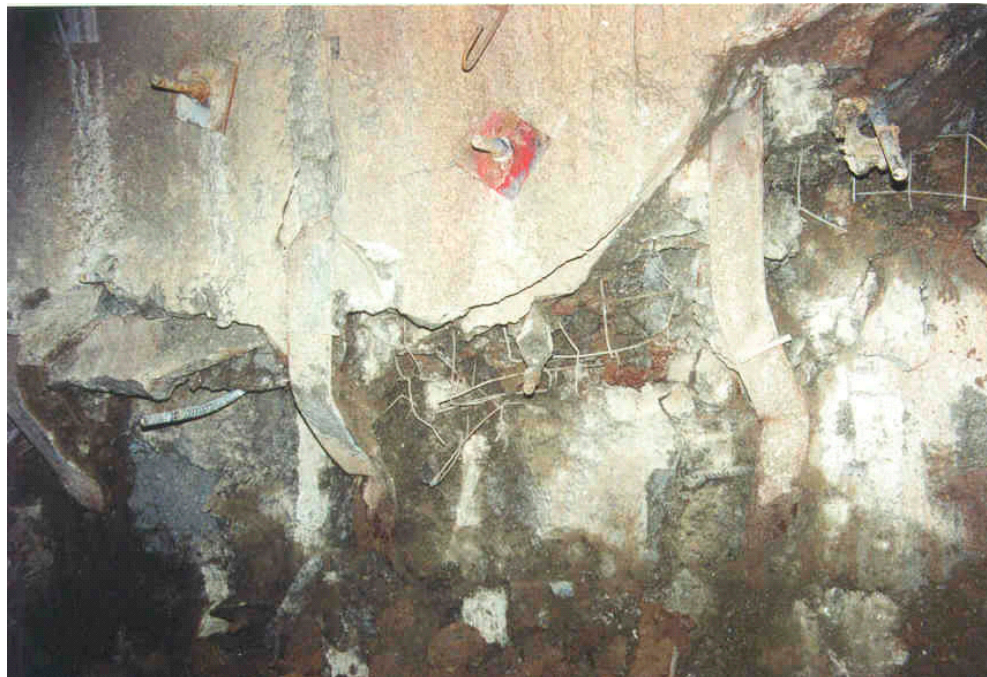


Figure 14. Displacement measurements at km: 64 + 172 in the left tunnel of Elmalık [51].

It is determined that the collapse in the Elmalık left tunnel (Figure 15) occurred in the fault zones, and serious problems were experienced in these sections before the earthquake

(Figure 15a). Moreover, deformations up to 100 cm took place in these sections accompanied with continuous strengthening and reinforcement studies (Figure 15b) [45,46,48].



(a)



(b)

Figure 15. Damage owing to the high deformations in the left tunnel lining (a) and the left tunnel reinforcement works (b) [45].

In the Elmalık right tunnel, the collapsed section formed between km: 54 + 060 and km: 54 + 160 was observed in 1996, because of extreme deformations reaching up to 1.3 m

(Figure 16), and, eventually, the tunnel completely collapsed (Figure 17). Afterwards, the section was excavated using the bench pilot tunnel method (Figure 12) [45,46,48].

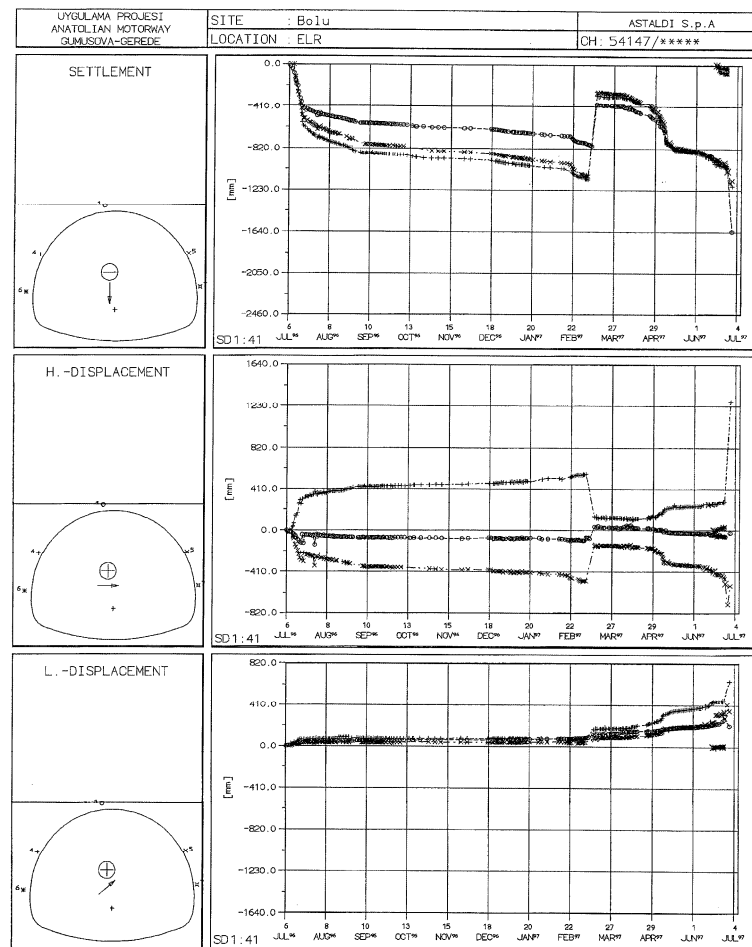


Figure 16. Right tunnel deformations at km: 54 + 147 [52].



Figure 17. The right tunnel collapse zone between 54 + 147 to 54 + 240 in 1996 (before the Düzce earthquake).

5. Analysis of Support Systems with Analytical Solutions and Evaluation of Tunnel Squeezing

It is important to examine the ground and support reaction curves and the squeezing conditions that will occur in the tunnel in order to evaluate the support systems in the flysch series. The rock mass parameters of the flysch series are presented in Table 2 [48].

Table 2. Rock mass parameters [48].

Deformation Modulus (MPa)	Uniaxial Compressive Strength (MPa)	Internal Friction Angle (ϕ) (Degree)	Unit Weight (kN/m^3)	Poisson Ratio (ν)	Overburden (m)
533	0.23	22	22	0.3	100

Hoek and Marinos (2000) [53] and Jethwa et al. (1984) [54] approaches were used to examine the tunnel squeezing. The equations for these approaches are presented in Table 3.

Table 3. Squeezing equations, according to Jethwa et al. (1984) [54] and Hoek and Marinos (2000) [53].

Researchers	Equations
Jethwa et al. (1984) [54]	$Nc = \frac{\sigma_{cm}}{P_0} = \frac{\sigma_{cm}}{\gamma * h}$ (1)
Hoek and Marinos (2000) [53]	$\mathcal{E} = 0.2 * (\sigma_{cm} / P_0)^{-2}$ (2)

σ_{cm} : uniaxial compressive strength of rock mass. h: overburden. γ : unit weight. P_0 : in situ stress.

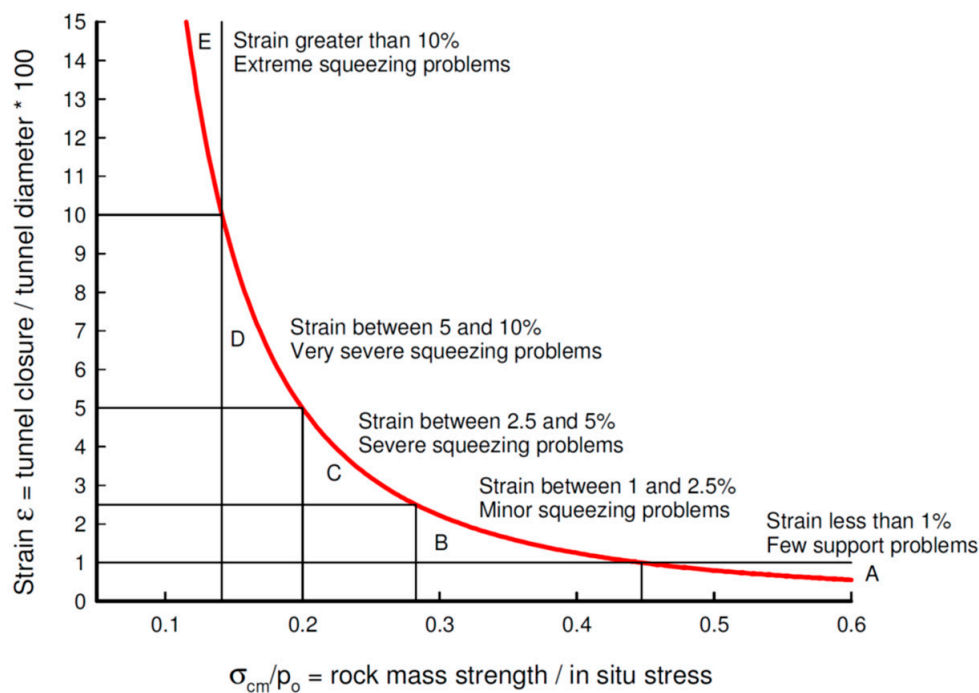
According Jethwa et al. (1984) [54], the Nc value was found to be 0.1, meaning that a high rate of squeezing would occur (Table 4). According to Hoek and Marinos (2000) [53], the \mathcal{E} value is calculated as 18%. As seen in Figure 18, it is stated that very serious stability problems will be encountered in the tunnel.

Table 4. Squeezing conditions according to Jethwa et al. (1984) [54].

Squeezing Conditions	Range
High	<0.4
Middle	0.4–0.8
Light	0.8–2
No squeezing	>2

The equations given by Hoek and Brown (1980) [55] and Hoek (2012) [56] are utilized to plot the ground reaction curve. These equations are presented in Table 5.

In the analyses, the radius of the plastic zone around the tunnel is 38 m, the σ_{cm}/P_0 ratio is 0.07, the critical pressure P_{cr} 1.20 MPa, and the total deformation is calculated as 55 cm (Table 6) (Figure 19).



	Strain ϵ %	Geotechnical issues	Support types
A	Less than 1	Few stability problems and very simple tunnel support design methods can be used. Tunnel support recommendations based upon rock mass classifications provide an adequate basis for design.	Very simple tunnelling conditions, with rockbolts and shotcrete typically used for support.
B	1 to 2.5	Convergence confinement methods are used to predict the formation of a 'plastic' zone in the rock mass surrounding a tunnel and of the interaction between the progressive development of this zone and different types of support.	Minor squeezing problems which are generally dealt with by rockbolts and shotcrete; sometimes with light steel sets or lattice girders are added for additional security.
C	2.5 to 5	Two-dimensional finite element analysis, incorporating support elements and excavation sequence, are normally used for this type of problem. Face stability is generally not a major problem.	Severe squeezing problems requiring rapid installation of support and careful control of construction quality. Heavy steel sets embedded in shotcrete are generally required.
D	5 to 10	The design of the tunnel is dominated by face stability issues and, while two-dimensional finite analyses are generally carried out, some estimates of the effects of forepoling and face reinforcement are required.	Very severe squeezing and face stability problems. Forepoling and face reinforcement with steel sets embedded in shotcrete are usually necessary.
E	More than 10	Severe face instability as well as squeezing of the tunnel make this an extremely difficult three-dimensional problem for which no effective design methods are currently available. Most solutions are based on experience.	Extreme squeezing problems. Forepoling and face reinforcement are usually applied and yielding support may be required in extreme cases.

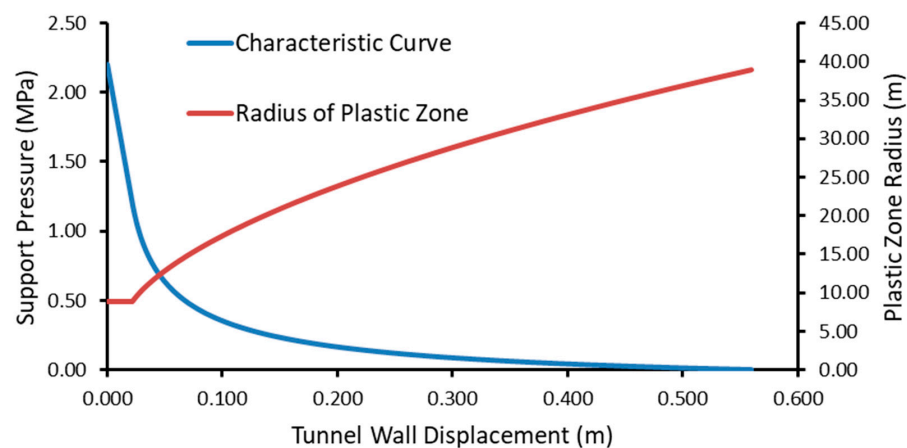
Figure 18. Squeezing conditions in the unsupported tunnel section [53].

Table 5. Closed form solution equations [55,56].

The uniaxial compressive strength of the rock mass σ_{cm} (3)	$\sigma_{cm} = \frac{2c' \cos \phi'}{1 - \sin \phi'}$	The radius of the plastic zone r_p when $p_i = 0$ (6)	$r_p = r_o \left[\left(\frac{2(p_0(k-1) + \sigma_{cm})}{(1+k)((k-1)p_i + \sigma_{cm})} \right)^{\frac{1}{k-1}} \right]$
Critical support pressure p_{cr} (4)	$p_{cr} = \frac{2p_0 - \sigma_{cm}}{1+k}$	Inward radial displacement u_{ip} (7)	$u_{ip} = \left(\frac{r_o(1+\phi)}{E_m} \right) [2(1-\phi)(p_0 - p_{cr}) \left(\frac{r_p}{r_o} \right)^2 - (1-2\phi)(p_0 - p_i)]$
Radial elastic displacement u_{ie} (5)	$u_{ie} = \frac{r_o(1+\phi)(p_0 - p_i)}{E_m}$	Per cent strain, ϵ (8)	$\epsilon\% = x100 = [0.2 - 0.25 \left(\frac{p_i}{p_0} \right) \left(\frac{\sigma_{cm}}{p_0} \right)^{2.4 \left(\frac{p_i}{p_0} \right) - 2}]$
r_p = plastic zone radius u_i = tunnel sidewall deformation r_o = original tunnel radius in metres p_i = internal support pressure p_o = in situ stress = depth below surface * unit weight of rock mass = $p_o = \gamma * h$			
σ'_1 = the axial stress at which failure occurs σ'_3 = the confining stress c' = the cohesive strength ϕ' i ϕ' = the angle of friction of the rock mass E_m = Young's modulus or deformation modulus ν = Poisson's ratio			

Table 6. Analytical solution results.

Rock Mass Strength σ_{cm}	In Situ Stress P_0	σ_{cm}/P_0	Plastic Zone Radius r_p (m)	Strain ϵ (%)	Total Deformation u_i (m)	Tunnel Face Deformation u_{if} (m)	Critical Support Pressure P_{cr} (MPa)
0.16	2.2	0.07	39	18	0.055	0.10	1.20

**Figure 19.** Characteristic curve and radius of the plastic zone.

In addition, the equations established by Vlachopoulos and Diedrichs (2009) [57] are used to plot the longitudinal deformation curve of the tunnel. The displacements obtained here increase rapidly towards the back of the tunnel face and reach up to 55 cm (Figure 20).

$$u^* = \frac{u}{u_{max}} = u_0^* e^{X^*} \quad (9)$$

for $X^* \leq 0$ (in the rock mass)

$$u^* = 1 - (1 - u_0^*) e^{-\frac{3X^*}{2R^*}} \quad (10)$$

for $X^* \geq 0$ (in the tunnel), where $R^* = R_p/R_T$

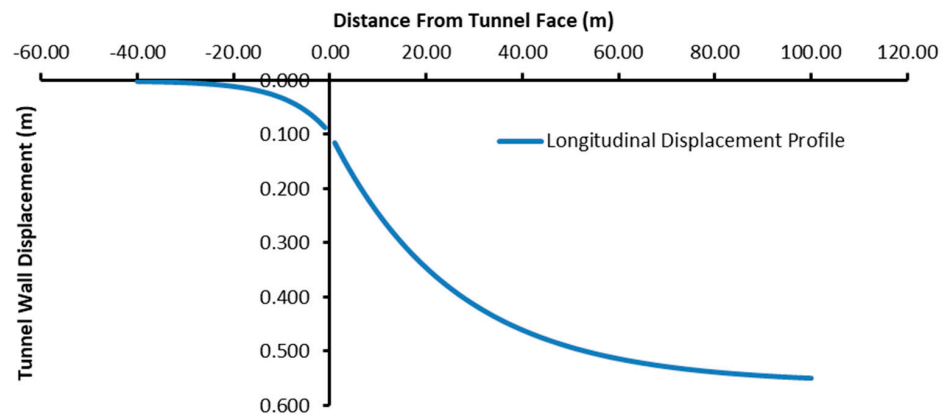


Figure 20. Longitudinal displacement profile.

The equations given by Brady and Brown (1985) [58] are used to determine the carrying capacity of the support systems used in the tunnel for drawing the support reaction curve. The support elements used in the flysch series are summarized in Table 7.

Table 7. Support system details in the flysch series.

Shotcrete	Steel Rib	Bolt
45 cm	HEB 140	12 m

The support system pressure (P_{ssmax}) and stiffness (K_{ss}) determined for HEB 140 type steel rib are presented in Table 8. The support pressure and stiffness of the steel rib are calculated using Equations (11) and (12).

$$P_{ssmax} = \frac{A_s * \sigma_{ys}}{s_l * l_{ro}} \quad (11)$$

$$K_{ssmax} = \frac{E_s * A_s}{s_l * l_{ro}^2} \quad (12)$$

Table 8. HEB140-type steel rib properties, P_{ssmax} and K_{ssmax} .

A_s (m ²)	s_l (m)	E_s (Mpa)	σ_{ys} (Mpa)	P_{ssmax} (MPa)	K_{ss} (MPa/m)
Cross-sectional area	Spacing along the tunnel axis	Young's modulus of the steel rib	Yield strength of the steel	Support pressure	Stiffness
0.00496	1	207,000	365	0.203	12.96

The strength properties of C25/30-type shotcrete are presented in Table 9. The support system pressure P_{scmax} and stiffness K_{sc} of the shotcrete are presented in Equation (13) and Equation (14), respectively.

$$P_{scmax} = \frac{\sigma_{cc}}{s} * \left[1 - \frac{(r_o - t_c)^2}{r_o^2} \right] \quad (13)$$

$$K_{sc} = \left(E_c * \frac{r_o^2 - (r_o - t_c)^2}{2 * (1 - \theta^2) * (r_o - t_c) * r_o^2} \right) \quad (14)$$

Table 9. C25/30-type shotcrete properties, P_{scmax} and K_{scmax} .

t_c (m)	ν_c	E_c (Mpa)	σ_{cc} (Mpa)	P_{scmax} (MPa)	K_{sc} (MPa/m)
Thickness of the shotcrete	Poisson ratio	Young's modulus of the shotcrete	Uniaxial compressive strength of the shotcrete	Support pressure	Stiffness
0.45	0.2	30,000	25	1.232	182.26

The properties of the bolts used in the tunnel are presented in Table 10. The support pressure P_{sbmax} and stiffness K_{sb} values of the bolts are shown in Equations (15) and (16).

$$P_{sbmax} = \frac{Tbf}{sl * sc} \quad (15)$$

$$K_{sb} = Es * \pi * \frac{db^2}{4slsc} \quad (16)$$

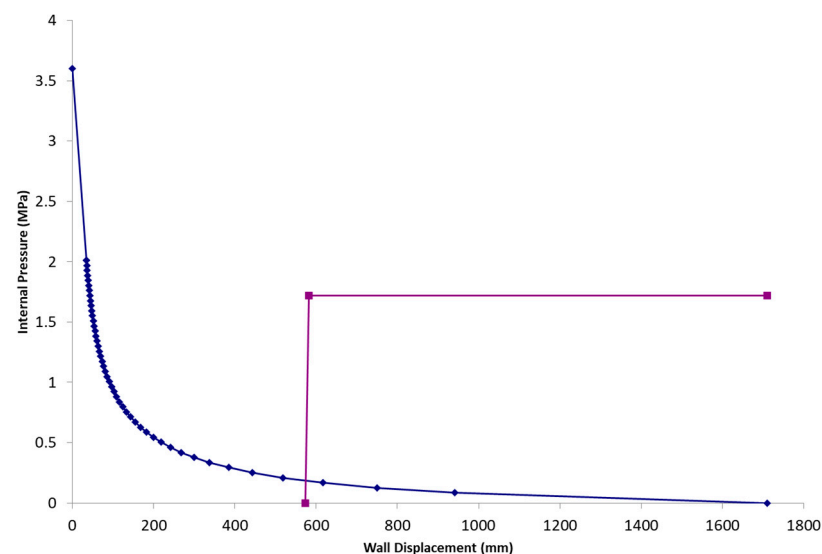
Table 10. Bolts properties, P_{sbmax} and K_{sbmax} .

d_b (m)	l (m)	E_s (Mpa)	s_c (m)	s_l (m)	T_{bf} (MN)	P_{sbmax} (MPa)	K_{sb} (Mpa/m)
0.032	12	207,000	1	1	0.280	0.28	13.87

The total support pressure system is calculated as $P_t = P_{sbmax} + P_{scmax} + P_{ssmax} = 1.71$ MPa. The critical pressure (P_{cr}) for the tunnel support system is determined as 1.20 MPa with the help of Equation (4).

Herein, the factor of safety is the ratio of P_{sm} (maximum support pressure) to the P_{eq} (equilibrium pressure).

The drawing of the ground and support reaction curves of the tunnel is evaluated in three stages. In the first stage, the situation where the supports were placed from 1 m behind the tunnel face was examined, and, further, it was observed that 526.67 mm deformation occurred in the tunnel face and 574.13 mm deformation in the tunnel (Figure 21). Although the safety factor is calculated as 9.34, it is known that the tunnel will fail because of deformations.

**Figure 21.** Support systems installed 1 m behind, FS:9.34, final wall displacement, 574.13 mm, and displacement at tunnel face, 526.67 mm.

Considering that the supports are placed without deformations in the second stage, the safety factor becomes 0.59, implying that the tunnel is not stable (Figure 22).

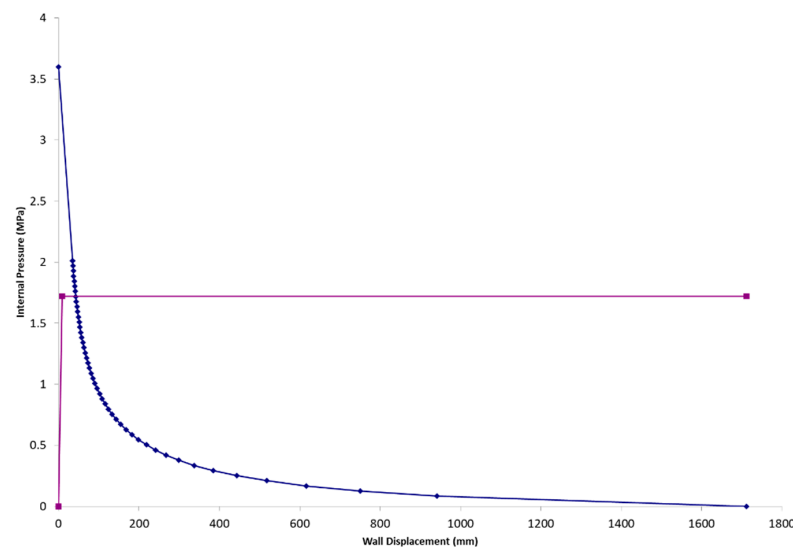


Figure 22. Tunnel support systems installed without deformation, FS:0.59, and final wall displacement 49.48 mm.

According to analysis, it was not possible to reach stability with the outer lining made in the tunnel. This fact sheds light on the problems experienced in the tunnel. Stability around the tunnel could not be achieved depending solely on the flexible outer lining. It has been observed that the deformations occurring in the flysch series of the tunnel exceeded 100 cm in places. The reason for these deformations is both insufficient external support and deformations that develop due to squeezing in the long term. After the problems experienced in the Bolu tunnel, intermediate lining (Bernold lining) was begun to be applied to the flysch series. The Bernold lining was begun to be installed from approximately 30 m behind the tunnel face, immediately after the outer lining, and stability was ensured in the tunnel. The properties of the Bernold lining are given in Table 11. The analyses are considered together with the outer lining and the intermediate lining. In this case, since the strength of the outer lining is $P_{\text{outer}} = 1.71$ MPa and $P_{\text{bernold}} = 1.62$ MPa, the total becomes $P_{\text{outer}} + P_{\text{bernold}} = 3.33$ MPa. The ground–support reaction curve is presented in Figure 23. Here, if there is a total deformation of 5 cm in the tunnel, the safety factor is 1.53. In fact, this is an extremely important approach in terms of ensuring the stability of the tunnel. This application was applied in the Bolu tunnel and produced successful results. In addition, no damage occurred in these parts of the tunnel during the 12 November 1999 Düzce earthquake. The sections where damage and collapse occurred were the sections with only the outer lining without the Bernold lining. In a sense, tunnel stability had been ensured with rigid lining. Hence, the main principle of NATM, a flexible outer lining, has failed.

Table 11. C25/30-type Bernold lining properties, P_{scmax} and K_{scmax} .

t_c (m)	ν_c	E_c (Mpa)	σ_{cc} (Mpa)	P_{scmax} (MPa)	K_{sc} (MPa/m)
Thickness of the Bernold lining	Poisson ratio	Young's modulus of the Bernold lining	Uniaxial compressive strength of the shotcrete	Support pressure	Stiffness
0.60	0.2	30,000	25	1.62	245.26

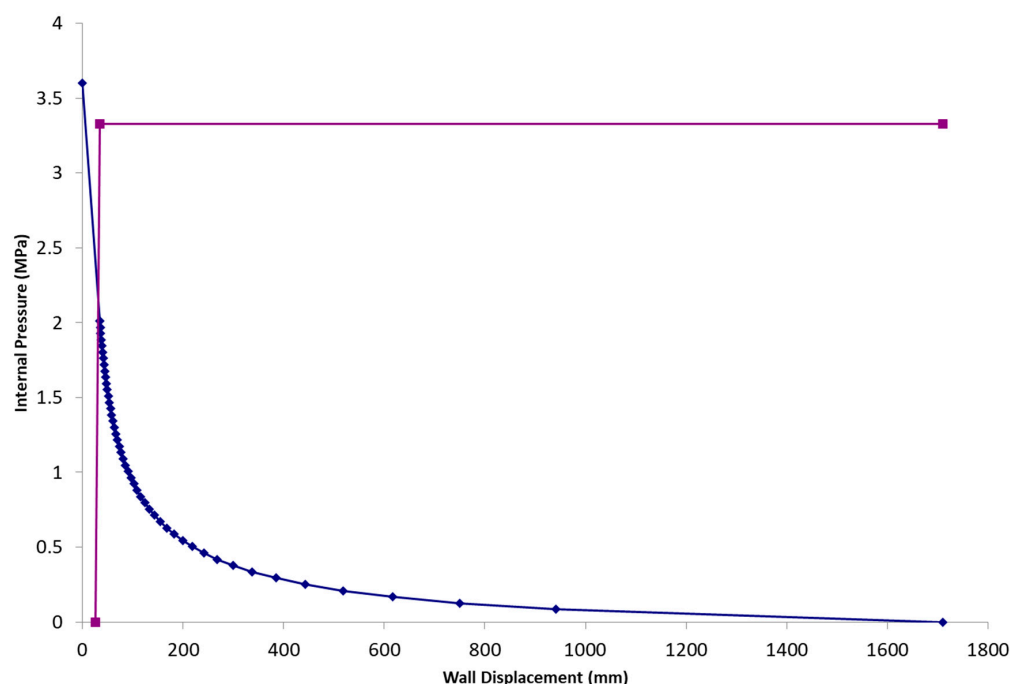


Figure 23. In the case where the support systems are placed before deformations occur in the tunnel, 1 m behind, FS:1.59, and final wall displacement, 30.81 mm.

6. The Impact of the Earthquake on the Bolu Tunnel

The Düzce earthquake on 12 November 1999 had a considerable impact on the Bolu tunnels. The 7.2 magnitude earthquake had a maximum horizontal ground acceleration value of 0.82 g, while the acceleration values for the Bolu tunnels are unknown. The study conducted by Durukal (2002) [59] estimated maximum accelerations based on the records of strong ground motion obtained from the Düzce and Bolu stations [44]. Several observations were performed through examinations conducted at the Asarsuyu entrance of the tunnel. No surface fractures were observed along the tunnel route [32]. It is believed that the instances of earthquake-related damage in the tunnel were caused only by shaking [60]. According to Hashash et al. (2001) [3], it is stated that tunnels opened in soil cause more disturbance than tunnels opened in solid rock. This situation is actually because the amplitudes and dominant vibration periods of the earthquake waves increase on the ground, causing more damage to the structure by creating a semi-resonance event [61]. For this reason, it increases the amplitudes and vibration periods of the earthquake wave in the clay units located in the fault zone. No damage was observed within 5.8 m diameter of the pedestrian tunnel, which was in a section supported by 30 cm thick shotcrete lining. Instances of superficial damage were observed at the inner lining of the construction joints between the paving blocks, which were 13.5 m long (1–5 mm wide). In addition, in the opening of the joints, thin non-structural cracks were observed that had formed in the tunnel, along with cavities in the corners. In the tunnel sections supported by shotcrete, a minimal level of damage was observed in the 16.5 m diameter of the main tunnels, which were supported by 45 cm of shotcrete lining over weak ground. In the metasediment series, spalling and longitudinal cracks were observed along with low to medium levels of damage in the bench and top-heading sections. Apart from this, no damage occurred that would adversely affect tunnel stability.

6.1. Investigation of the Collapsed Sections in the Elmalık Sections

After the collapse in the tunnel, boreholes were drilled in the left and right tunnels to clearly examine the tunnel condition and assess the current situation. A total number of 11 boreholes were drilled in the left and right tubes, as presented in Figure 24.

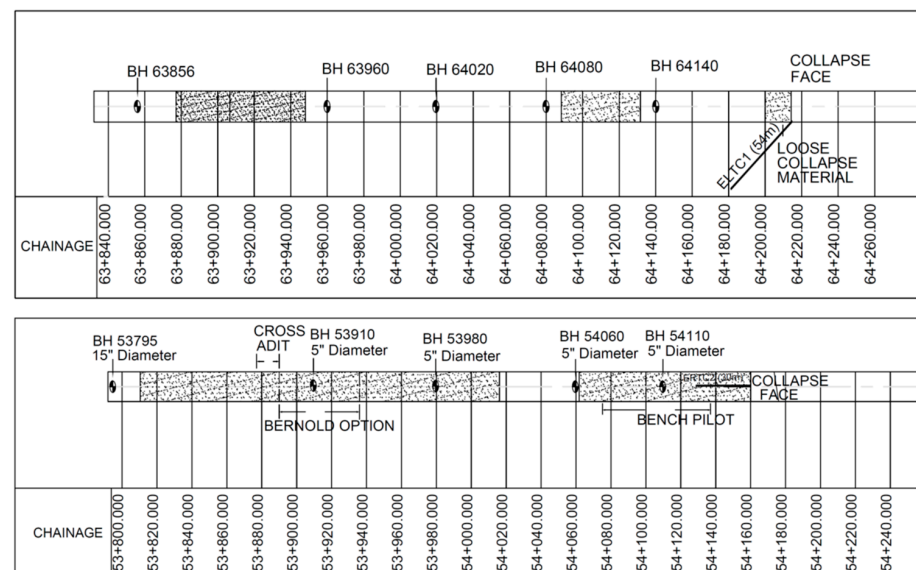


Figure 24. Locations of boreholes and collapse.

Among those, 2 had a diameter of 20 cm, whereas 9 had a diameter of 12.7 cm. The purpose of the boreholes of 20 cm diameter was to determine the current ground condition and to drain the water in the tunnels. The drillings in the left tunnel at km: 63 + 856.5 revealed the surface settlement occurred at km: 63 + 860 and had turned into a sinkhole formation (Figure 25).



Figure 25. Sinkhole above the tunnel alignment [12].

According to the field studies and horizontal and vertical drillings, it has clearly been seen that a 200 m section of the tunnel had completely collapsed. In addition, a sinkhole was observed at km: 63 + 860 on the left tunnel whose depth reached up to 20–30 m. This sinkhole had widened towards the right tunnel. This sinkhole indicated the existence of another collapse in the tunnel, that is, between km: 63 + 875 and km: 63 + 935.

Consequently, this borehole could not be studied. The borehole at km: 53 + 795 in the right tunnel coincided with a collapse [62]. The geometry of the collapse in the tunnel was expected to be identified by using the boreholes in the right tunnel. In the boreholes drilled at km: 53 + 910, a collapse was observed between 94.0 and 104.0 m depths. In the borehole of km: 53 + 980, the collapsed area reached between 70.0 and 82.0 m. At km: 54 + 060, it was identified that the tunnel ceiling was closed for almost 2.0 m while the tunnel entirely filled with collapsed material, and, in turn, settlements were observed in the surface topography. At km: 54 + 110, a collapse was encountered between 39.0 and 58.0 m depth. In the boreholes in the left tunnel, no collapse was observed at km: 63 + 791.5, km: 63 + 960, and km: 64 + 020 drillings. It was observed that inside the tunnel it was filled with loose material at km: 64 + 080. At km: 64 + 140 borehole, a collapse was encountered between 36.0 and 72.0 m depths. In addition to the vertical boreholes, two horizontal boreholes were also drilled in both tubes. As a result of this research and these evaluations, the collapsed sections are modeled and presented in Figures 26 and 27.

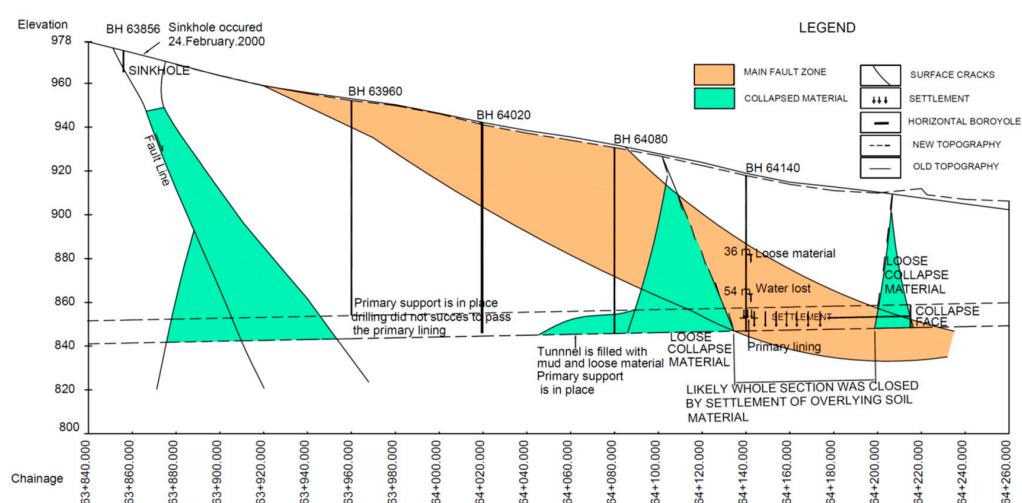


Figure 26. Left tunnel longitudinal section after the 12 November 1999 Düzce earthquake [63].

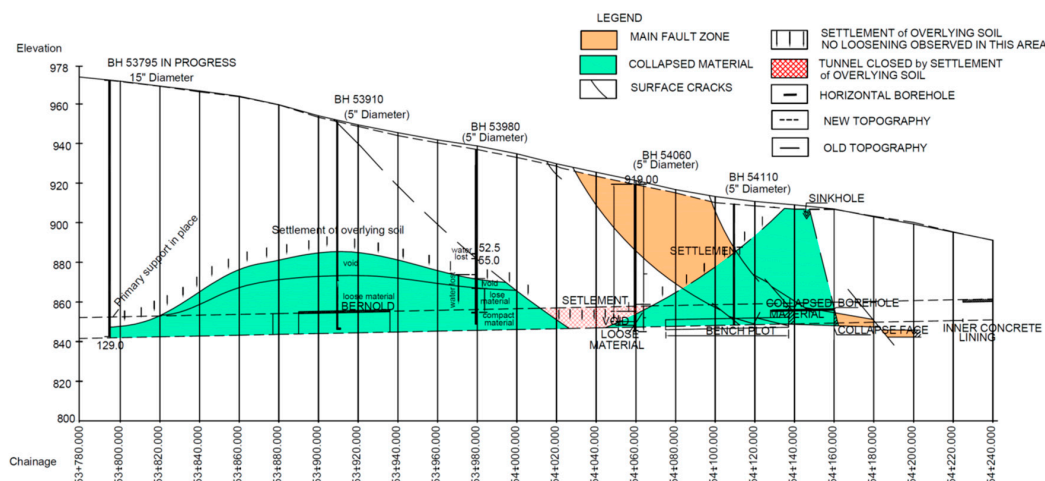


Figure 27. Right tunnel longitudinal section after the 12 November 1999 Düzce earthquake [63].

6.2. Investigation of the Collapsed Sections in the Asarsuyu Sections

Severe deformations were observed in clay units inside the bench pilot tunnels that were excavated at the Asarsuyu entrance through faults [32]. Buckling at steel arches up to 30–40 cm was observed. Swelling at the invert of 0.5 m and 1.0 m were detected (Figure 28).

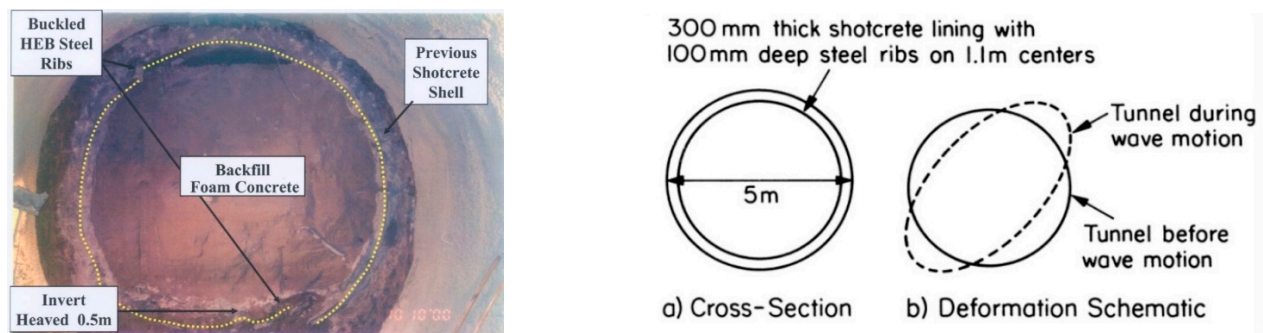


Figure 28. View of the collapsed tunnel after it had been re-excavated and back-filled with foam concrete [8] and bench pilot tunnel cross-section and seismic distortion [32].

In addition, tension cracks oriented towards the axis and shear cracks extending from the axis to the sides were observed at the invert sections constructed in the left and right tunnels of the Asarsuyu entrance. The cracks' widths varied from 0.005 cm to 0.01 cm. In accordance with the examinations conducted at the Asarsuyu entrance, no cracks were encountered in the Option 3 support system (Bernold Lining method) applied in the Bakacak fault, which is the most critical place. Eventually, it was noted that the applied Option 3 support system can withstand the earthquake load [64].

The greatest impact of the earthquake was on the tunnel's Elmalık entrance, causing instances of collapse inside the tunnel at approximately 400 m from the entrance. It was observed that the instances of collapse on the Elmalık side developed in the tunnel sections where there is no inner lining, and the deformation stabilized (Figure 29). In contrast, no damage was sustained in an approximate 400 m section where the inner lining was already installed, and the deformations were under 2 mm/month. At the portal entrance of Elmalık (east portal), stability of the tunnel could not be achieved, even in static condition. In other words, even before the earthquake, deformations up to 1.0 m occurred in the sections where the collapse occurred. During the earthquake, the extra earthquake loads caused the tunnel to collapse. Following the Düzce earthquake, in the Elmalık area where the fault zone passed over the surface, large cracks and settlements were identified on the ground due to the collapse [32,65]. A cone-shaped subsidence with a diameter of 9–10 m was formed in the right tunnel, and, later, another large subsidence with a diameter of 15–20 m was formed at km: 63 + 860 in the left tunnel [32]. Furthermore, 4.5 months after the earthquake, a sinkhole with a diameter of 8 m formed beneath the overburden thickness of 122 m. Therefore, it can be understood that the collapse in the tunnel has progressed towards the surface.

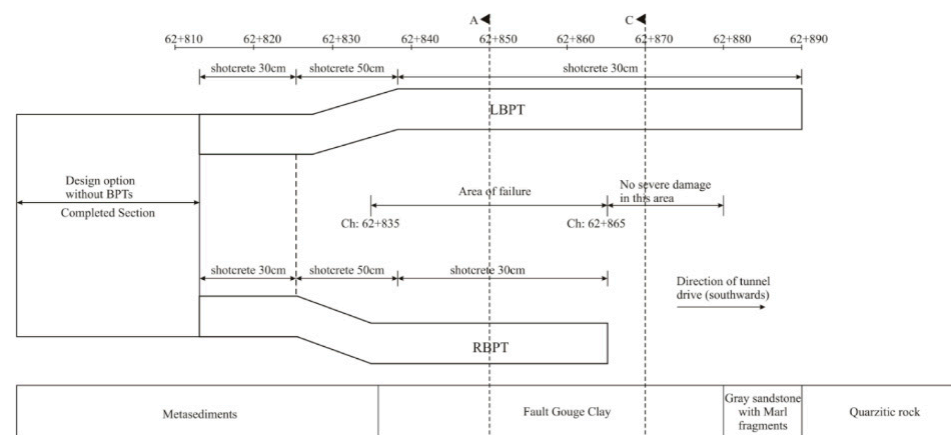


Figure 29. Plan view of the Asarsuyu left drive showing the main tunnel and the two bench pilot tunnels under construction at the time of the earthquake [8].

6.3. Evaluation of Geotechnical Measurements in the Tunnel after the 12 November 1999 Düzce Earthquake

Geotechnical measurement instruments were placed throughout the normal excavation of the Bolu tunnel, including the Asarsuyu and Elmalık entrances. However, due to the collapse of the Elmalık entrance during the earthquake, measurements could not be ascertained at this section. As there were no instances of collapse at the Asarsuyu entrance, measurements could be obtained at this section. The results obtained using the geotechnical measurement instruments that were placed within the inner lining at the Asarsuyu entrance of the tunnel are discussed below. The geotechnical measurements obtained from the inner lining of the Asarsuyu tunnel (61st block km: 62 + 005 and 62 + 018) are investigated. The depth of this section from the surface is approximately 200 m, which is in the metacrystalline layer. C2M class support is applied to this section. The measurements from this section included measurements taken before and after the Düzce earthquake.

Measurements were taken for this section because results could still be obtained as the Düzce earthquake did not cause any damage here. Figure 13 shows the images during the utilization of the geotechnical measurement instruments. The pressure cells are positioned in the tunnel in a tangential and radial manner, while the unit deformation gauges are placed near the two concrete surfaces.

The results obtained from the geotechnical measurement instruments placed in the concrete inner lining at the Asarsuyu entrance of the tunnel are shown in Figures 24 and 26. In this section, the results obtained both before and after the earthquake were examined to determine any changes that might have occurred in the inner lining's bending moments, forces, stresses, and unit deformations during the earthquake.

The deformation-related changes that occurred in this section during the earthquake have been summarized, as follows: in Section 1, no significant difference could be noted at the inner part before and after the earthquake, while a decrease of 210 $\mu\text{m}/\text{m}$ was observed in its outer part; in Section 2, a decrease of 140 $\mu\text{m}/\text{m}$ occurred in the inner part, while a decrease of 116 $\mu\text{m}/\text{m}$ occurred in the outer part; in Section 3, a 153 $\mu\text{m}/\text{m}$ decrease was noted in the inner part, while no measurement could be obtained from the outer part; in Section 4, no reading was obtained from the inner part, while an increase of 35 $\mu\text{m}/\text{m}$ was measured in the outer part; and in Section 5, there is a decrease of 355 $\mu\text{m}/\text{m}$ in the inner part and an increase of 60 $\mu\text{m}/\text{m}$ in the outer part (Figure 30).

The changes that occurred in the normal forces and bending moment acting on the concrete inner lining after the earthquake are summarized as follows: there is an increase of 1240 MN in Section 1 and an increase of 1360 MN in Section 2, while no readings could be obtained from Section 3; there is also an increase of 4 MN in Section 4 and 1.54 MN in Section 5 in axial force measurements (Figure 31).

While no reading could be obtained from Section 4, there is an increase of 0.15 MN/m in Section 1, a decrease of 0.14 MN/m in Section 2, and a decrease of 0.64 MN/m in Section 3. There is also decrease of 0.41 MN/m in Section 5 in bending moments.

From the monitoring readings obtained from pressure cells placed in Section 1, it was observed that the stresses increased up to 15 MPa around the lining during the earthquake (Figure 32), and the maximum change identified was occurred at the ceiling point. As shown in Figure 32, based on the measurements taken at the intersection of the top-heading and bench, the stress values are determined to be approximately 20 MPa.

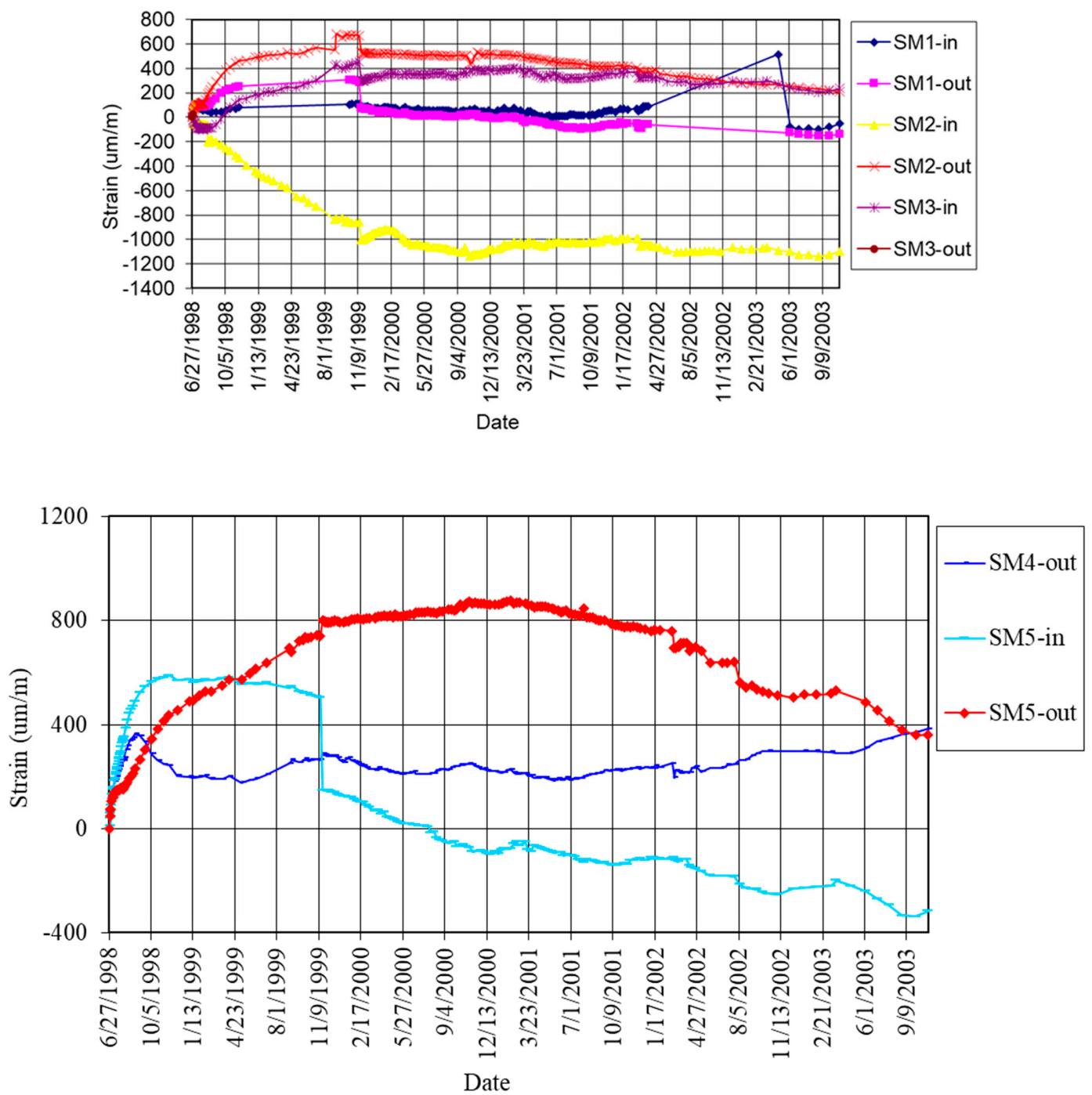


Figure 30. Unit deformations in the concrete inner lining (points 1, 2, 3, 4, and 5) at the 61st block of the left tunnel of Asarsuyu [66].

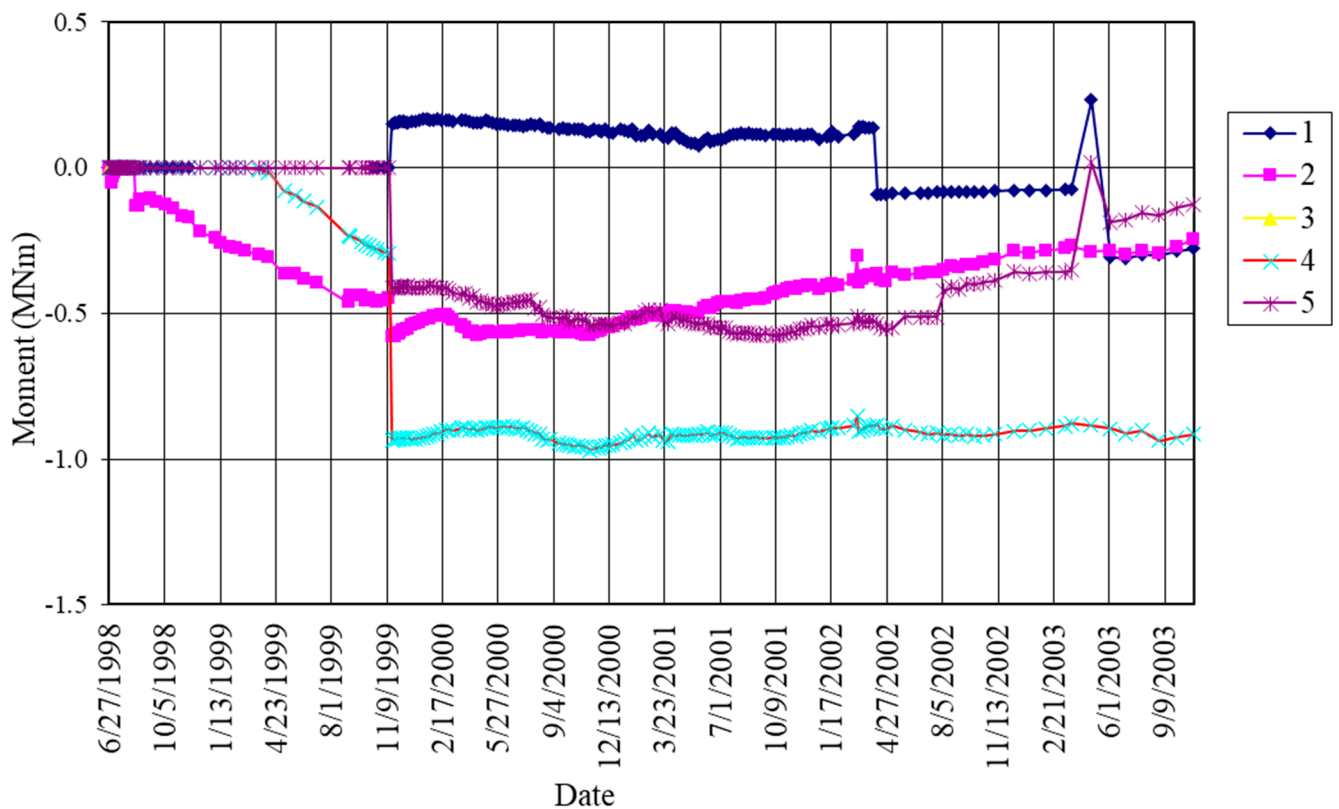
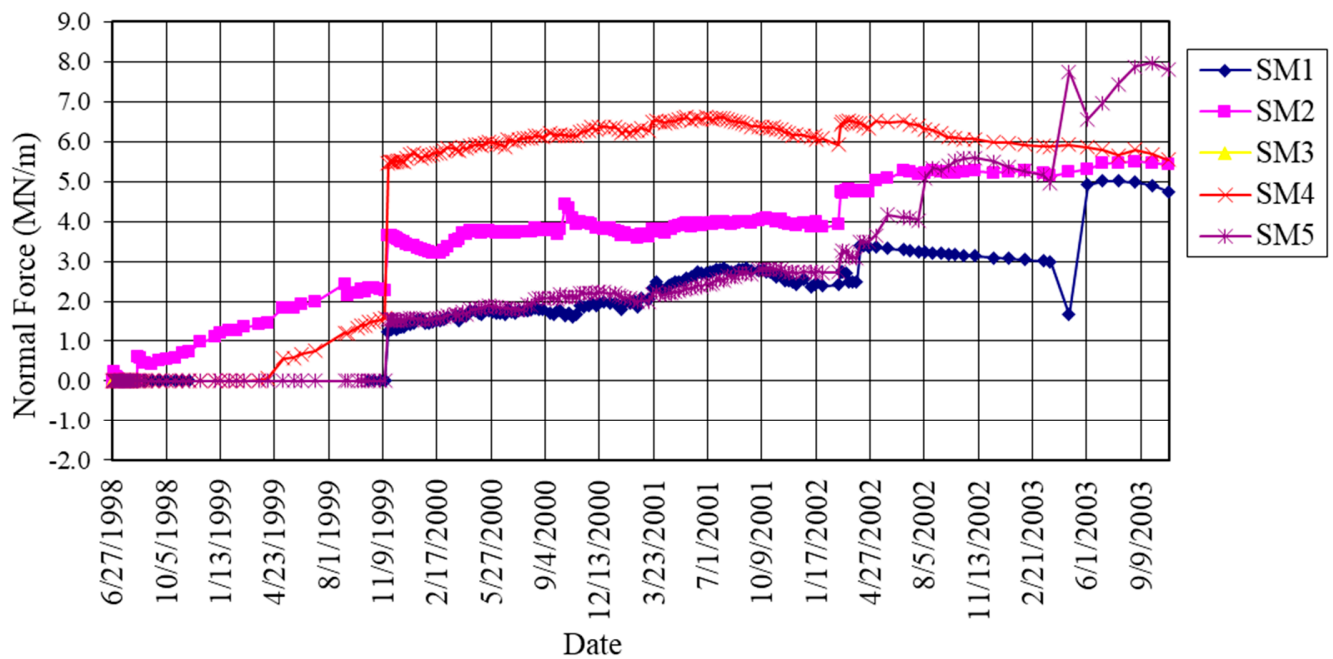


Figure 31. Normal forces and bending moment acting on the concrete inner lining at the 61st block in the left tunnel of Asarsuyu [66].

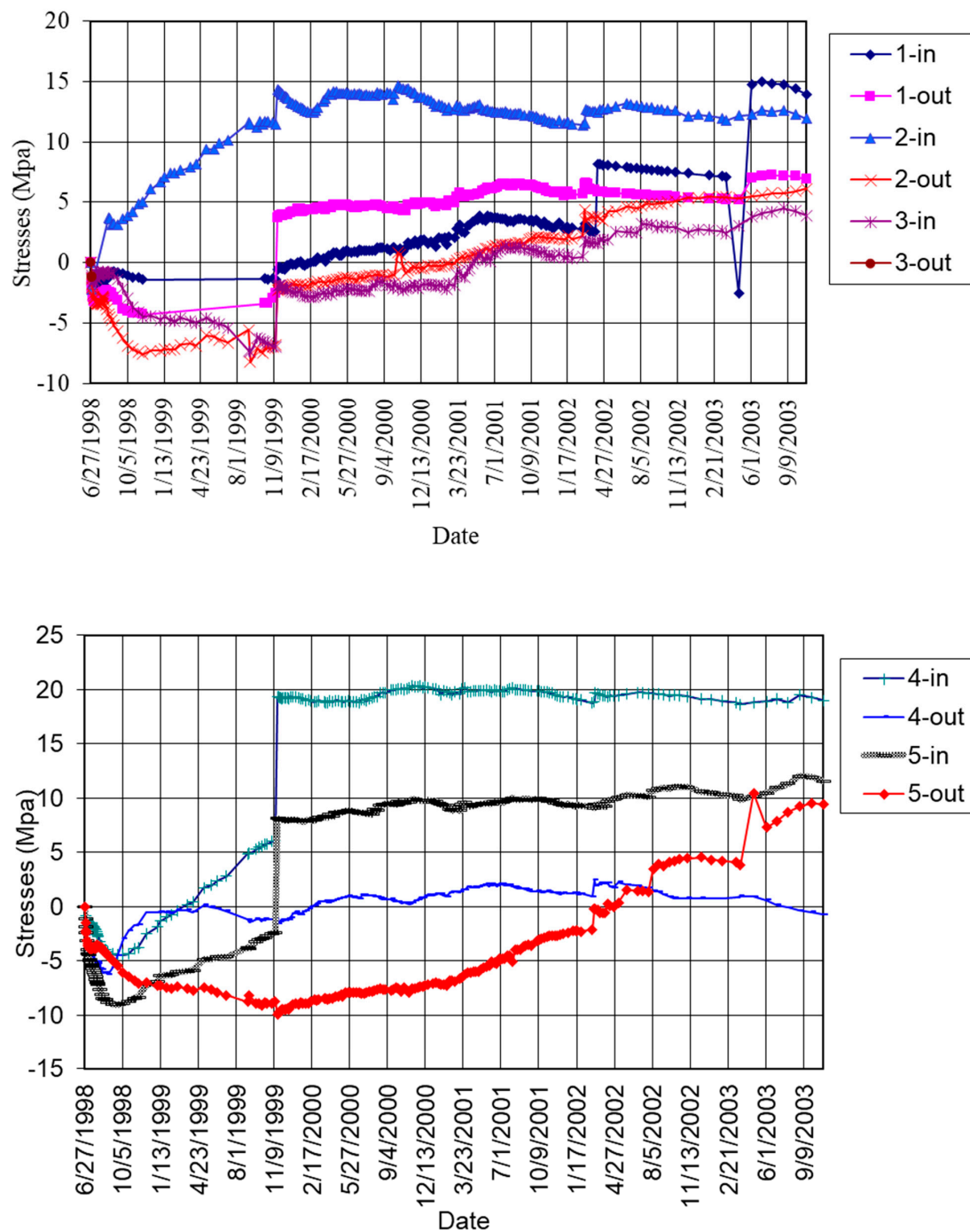


Figure 32. Stresses that occurred in the concrete inner lining (point 1, 2, 3, 4, and 5) at the 61st block of the left tunnel of Asarsuyu [66].

Abrupt increases in the level of deformation, tension, bending moment, and force were observed after the earthquake. However, these changes did not cause any significant problems in the tunnel, as the support systems were able to carry the generated loads effectively. The change in deformations, stresses, bending moments, and force remained within limit values, and they normalized to reach inner stability after a period, as can be seen from the obtained results. In the Asarsuyu section of the tunnel, only minor cracks occurred in the inner lining, and these did not have any adverse effect on the tunnel's stability.

6.4. Inner Lining Design after the Düzce Earthquake

After the Düzce earthquake, Letis and Barka (2000) [31] reported that the active Bakacak fault has the potential to create a fault rupture that could cause a 30–50 cm displacement [67]. In order to minimize the damage to the tunnel from this potential displacement, a 50 cm wide gap was left in the inner lining every 4.4 m. These gaps were filled with aerated concrete (Figures 33 and 34), called seismic joints.



Figure 33. Seismic joints in the inner concrete lining.

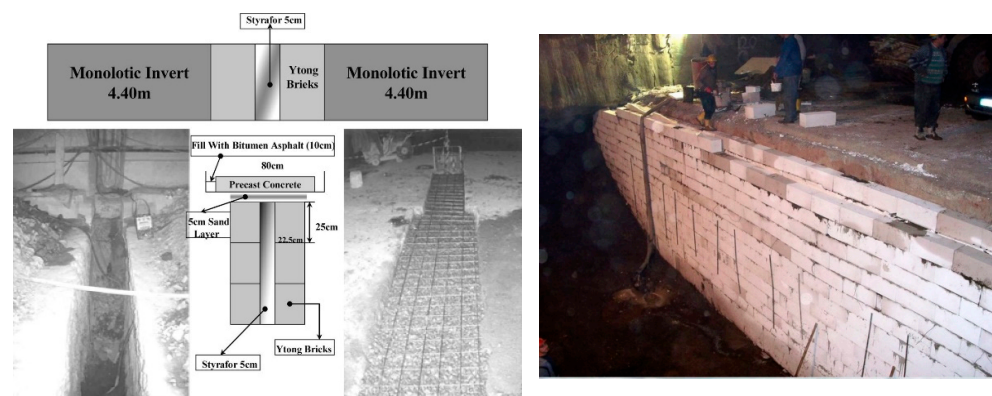


Figure 34. Detailed seismic joints in the monolithic invert [32] and seismic joints at the concrete invert [12].

In addition, the ring closure was provided along with the application of a rigid support system by installation of monolithic reinforced invert concrete after the invert excavation (Figure 35).



Figure 35. Application of invert with reinforced concrete.

7. Conclusions

It can be concluded that the section stability of the tunnels could not be achieved even before the earthquake where the collapse occurred at the entrance of Elmalık portal. Deformations exceeding 1.5 m occurred in this region. The earthquake was not the main cause of this collapse; it only had a triggering effect.

The collapse did not occur after the earthquake, but after the failure of the support systems due to the aftershocks that took place two to three days after the earthquake.

Furthermore, it is known that in the Asarsuyu entrance, which has good rock conditions, no serious damage occurred at the tunnel sections where the inner lining had been installed. Moreover, even the sections with no inner lining exhibited only minor fractures.

Therefore, it is necessary that the inner linings are always reinforced in shallow tunnels that are surrounded by weak ground and located in areas with high earthquake risk.

The inner concrete lining should be designed according to the earthquake loads. The construction of the inner lining immediately after the top-heading, bench, and invert excavations is extremely vital to ensure the stability of the tunnels in weak ground conditions.

It is understood from the example at the Bolu tunnel that load implied from the earthquake has practically no destructive effect itself on deep tunnels and those surrounded by rock units, especially in the case of the Asarsuyu entrance.

Moreover, earthquakes may have no destructive effects on sections of tunnels where the tunnel stability is ensured, and the inner lining is properly installed.

In large-diameter tunnels excavated in weak soils under high overburden pressure, a rigid lining is required instead of a flexible outer lining to ensure tunnel stability. The critical pressure of the support system was calculated as 1.20 MPa.

The support system pressure, which provides a safety factor of 1.5, was found to be 3.30 MPa. The ratio between the support system pressure and the critical pressure was 2.75. Therefore, the pressure of the tunnel support systems should be 2.75 times the critical pressure to ensure tunnel stability in weak ground.

The basic principle of NATM, a flexible outer lining principle, is out of date for large-diameter tunnels excavated in weak soils, and needs to be revised. This principle should be changed to rigid lining in weak ground. Inner lining should be designed with seismic joints to reduce damage from earthquakes in fault zones.

8. Discussion

According to the results, the tunnel lining design should be carrying the load due to the earthquake in the fault zones. If the fault rupture causes the unavoidable displacement, a gap should be left in the inner lining.

In the fault zones, the ring closure (top heading, bench, and invert excavations) and inner lining should be installed as soon as possible to avoid unexpected loads and to prevent instability in the long term.

Another important factor is to select the tunnel route. If there is a possibility, the tunnel alignment should be selected far from fault zones.

Funding: This research received no external funding.

Institutional Review Board Statement: Not applicable.

Informed Consent Statement: Not applicable.

Data Availability Statement: All data generated or analyzed during this study are included in this published article.

Acknowledgments: The authors would like to thank the General Directorate of Highways of Turkey for the data support.

Conflicts of Interest: The author declares no conflict of interest.

References

1. St-John, C.M.; Zahrah, T.F. Asiesmic Design of Underground Structures. *Tunn. Undergr. Space Technol.* **1987**, *2*, 165–197. [CrossRef]
2. Ghasemi, H.; Coor, J.D.; Imbsen, R.; Piskin, H.; İnal, F.; Tiras, A. The November 1999 Duzce Earthquake: Post-Earthquake Investigation of the Structures on the Term. Publication No: FHWA-RD-146; 1999; p. 26. Available online: <https://www.fhwa.dot.gov/publications/research/infrastructure/structures/00146.pdf> (accessed on 15 August 2023).
3. Hashash, Y.M.A.; Hook, J.J.; Schmidt, B.; Yao, J.I.C. Seismic design and analysis of underground structures. *ITA/AITES Accredited. Mater. Tunn. Undergr. Space Technol.* **2001**, *16*, 247–293. [CrossRef]
4. Wang, W.L.; Wang, T.T.; Su, J.J.; Lin, C.H.; Seng, C.R.; Huang, T.H. Assessment of damage in mountain tunnels due to the taiwan chi-chi earthquake. *Tunn. Undergr. Space Technol.* **2001**, *16*, 133–150. [CrossRef]
5. Elgamal, A.; Elfari, N. Adverse impact of earthquake seismic loading on angular offset tunnels and effects of isolation grout. *Infrastructures* **2022**, *7*, 87. [CrossRef]
6. Pakbaz, M.C.; Yareevand, A. 2-d analysis of circular tunnel against earthquake loading. *Tunn. Undergr. Space Technol.* **2005**, *20*, 411–417. [CrossRef]
7. Hwang, J.H.; Lu, C.C. Seismic capacity assessment of old Sanyi railway tunnels. *Tunn. Undergr. Space Technol.* **2007**, *22*, 433–449. [CrossRef]
8. Kontoe, S.; Zdravković, L.; Potts, D.M.; Menkiti, C.O. Case study on seismic tunnel response. *Can. Geotech. J.* **2008**, *45*, 1743–1764. [CrossRef]
9. Kontoe, S.; Zdravkovic, L.; Potts, D.; Mentiki, C. On the relative merits of simple and advanced constitutive models in dynamic analysis of tunnels. *Geotechnique* **2011**, *61*, 815–829. [CrossRef]
10. Kutter, B.L.; Chou, J.C.; Travararou, T. Centrifuge testing of the seismic performance of a submerged cut and cover tunnel in liquefiable soils. In Proceedings of the Fourth Geotechnical Earthquake Engineering and Soils Dynamics Conference (GEESDC), Sacramento, CA, USA, 18–22 May 2008.
11. Sedarat, H.; Kozak, A.; Hashash, Y.M.A.; Shamsabadi, A.; Krivotat, A. Contact interface in seismic analysis of circular tunnels. *Tunn. Undergr. Space Technol.* **2009**, *24*, 482–490. [CrossRef]
12. Brandl, J. Challenges to tunnel design a case history of the bolu tunnel. In Proceedings of the 2nd Expert Group Meeting, Ankara, Turkey, 2–3 April 2012.
13. Pitilakis, K.; Tsinidis, G.; Chalatis, A. Shallow immersed rectangular tunnel in soft soils. In *ISO/TR 12930:2014 Seismic Design Examples Based on ISO 23459*; International Organization for Standardization: Geneva, Switzerland, 2014.
14. Pitilakis, K.; Tsinidis, G. Performance and seismic design of underground structures. In *Earthquake Geotechnical Engineering Design*; Springer: Cham, Switzerland, 2014; pp. 279–340.
15. Kampas, G.; Knappett, J.A.; Brown, M.J.; Anastasopoulos, I.; Nikitas, N.; Alonso-Rodriguez, A.; Fuentes, R. Suitability of equivalent linear soil models for analysing the seismic response of a concrete tunnel. In Proceedings of the 16th European Conference of Earthquake Engineering, Thessaloniki, Greece, 18–20 June 2018.
16. Kampas, G.; Knappett, J.A.; Brown, M.J.; Anastasopoulos, I.; Nikitas, N.; Fuentes, R. The effect of tunnel lining modelling approaches on the seismic response of sprayed concrete tunnels in coarse-grained soils. *Soil Dyn. Earthq. Eng.* **2019**, *117*, 122–137. [CrossRef]
17. Tsinidis, G.; De Silva, F.; Anastasopoulos, I.; Bilotta, E.; Bobet AHashash, Y.M.A.; He, C.; Kampas, G.; Knappett, J.; Madabhushi, G.; Nikitas, N.; et al. Seismic Behavior of Tunnels: From Experiments to Analysis. *Tunn. Undergr. Space Technol.* **2020**, *99*, 103334. [CrossRef]
18. Patil, M.; Choudhury, D.; Ranjith, P.G.; Zhao, J. Behavior of shallow tunnel in soft soil under seismic conditions. *Tunn. Undergr. Space Technol.* **2018**, *82*, 30–38. [CrossRef]
19. Chao, M.; Dechun, L.; Xiuli, D. Seismic performance upgrading for underground structures by introducing sliding isolation bearings. *Tunn. Undergr. Sp. Tech.* **2018**, *74*, 1–9.
20. Lu, C.C.; Hwang, J.H. Nonlinear collapse simulation of Daikai Subway in the 1995 Kobe earthquake: Necessity of dynamic analysis for a shallow tunnel. *Tunn. Undergr. Space Technol.* **2019**, *87*, 78–90. [CrossRef]
21. Altunel, E.; Barka, A.A.; Çakır, Z.; Kozacı, Ö.; Hitchcock, C.; Helms, J.; Elms, J.; Bachhuber, J.; Lettis, W. What goes on at the eastern termination of the November 12, 1999 Düzce earthquake, M=7.2, North Anatolian Fault, Turkey. In Proceedings of the American Geophysical Fall Meeting, San Francisco, CA, USA, 15–19 December 2000; p. F816.
22. Ayhan, M.E.; Burgmann, R.; McCusky, S.; Lenk, O.; Aktu, B.; Herece, E.; Erece, E.; Reilinger, R.E. Kinematics of the Mw=7.2, 12 November 1999, Düzce, Turkey earthquake. *Geophys. Res. Lett.* **2001**, *28*, 367–370. [CrossRef]
23. Barka, A.A.; Altunel, E.; Akyüz, S.; Çakır, R.; Kozacı, O.; Lettis, W.; Bachhuber, J.; Hitchcock, C.; Helms, J. Seismic Activity and Fault Segmentation of the NAF in the Bolu Mountain: Relationship between the November 12, 1999 and the February 1, 1944 Earthquakes. In Proceedings of the EUG XI Meeting, Strasbourg, France, 8–12 April 2001; p. 295.
24. Akyuz, H.; Hartleb, S.R.; Barka, A.; Altunel, E.; Sunal, G.; Meyer, B.; Armijo, R. Surface rupture and slip distribution of the 12 november 1999 duzce earthquake, (m 7.1), north anatolian fault, Bolu, Turkey. *Bull. Seism. Soc. Am.* **2002**, *92*, 61–66. [CrossRef]
25. Bock, G.; Tibi, R.; Baumbach, M.; Grosser, H.; Milkereit, C.; Kind, R.; Zschau, J. Rupture processes of the August 17 İzmit and November 12, 1999 Düzce earthquakes. In *The 1999 İzmit and Düzce Earthquakes: Preliminary Results*; Barka, A.A., Kozacı, O., Akyüz, S., Altunel, E., Eds.; İstanbul Technical University Publication: İstanbul, Turkey, 2000; pp. 105–108.

26. Bouchon, M.; Bouin, M.-P.; Karabulut, H.; Toksöz, N.; Dietrich, M.; Rosakis, A.J. How fast is rupture during an earthquake? New insights from the 1999 Turkey earthquakes. *Geophys. Res. Lett.* **2001**, *28*, 2723–2725. [\[CrossRef\]](#)
27. Bouchon, M.; Toksoz, N.; Karabulut, H.; Bouin, M.P.; Dietrich, M.; Aktar, M.; Edie, M. Space and time evolution of rupture and faulting during the 1999 Izmit (Turkey) earthquake. *Bull. Seism. Soc. Am.* **2002**, *92*, 256–266. [\[CrossRef\]](#)
28. Bürgman, R.; Ayhan, M.A.; Fielding, E.J.; Wright, T.; McClusky, S.; Aktug, B.; Demir, C.; Lenk, O.; Türkezer, A. Deformation during the 12 November 1999, Düzce, Turkey Earthquake, from GPS and InSAR Data. *Bull. Seismol. Soc. Am.* **2002**, *92*, 161–171. [\[CrossRef\]](#)
29. Bouin, M.-P.; Bouchon, M.; Karabulut, H.; Aktar, M. Rupture process of the 1999 November 12 Duzce (Turkey) earthquake deduced from strong motion and Global Positioning System measurements. *Geophys. J. Int.* **2004**, *159*, 207–211.
30. Duman, T.Y.; Emre, O.; Dogan, A.; Ozal, S. Step-over and bend structures along the 1999 duzce earthquake surface rupture, North Anatolian Fault, Turkey. *Bull. Seismol. Soc. Am.* **2005**, *95*, 1250–1262. [\[CrossRef\]](#)
31. Lettis, W.; Barka, A. Geologic characterization of fault rupture hazard, Gumusova—Gerde Motorway. In *Report Prepared for the Astaldi-Bayindir Joint Venture Turkey*; Astaldi: Bolu, Turkey, 2000.
32. Ozben, M.; Tokgozoglu, F.; Isik, S. Seismic assessment results and actual application in the complex ground conditions of Bolu tunnels after the 1999 Duzce earthquake. In *Underground Space Use: Analysis of the Past and Lessons for the Future*; CRC Press: Boca Raton, FL, USA, 2005; pp. 657–662.
33. Dowding, C.H.; Rozen, A. Damage to rock tunnels from earthquake shaking. *J. Geotech. Eng. Div.* **1978**, *104*, 175–191. [\[CrossRef\]](#)
34. Rowe, R. Tunneling in seismic zones. *Tunn. Tunneling* **1992**, *24*, 41–44.
35. Wang, J.N. Seismic Design of Tunnels: A State-of-the-Art Approach. In *Monograph 7*; Parsons, Brinckerhoff Quade and Douglas Inc.: New York, NY, USA, 1993.
36. Aygar, E.B.; Gokçeoglu, C. Problems encountered during a railway tunnel excavation in squeezing and swelling materials and possible engineering measures: A case study from turkey. *Sustainability* **2020**, *12*, 1166. [\[CrossRef\]](#)
37. Aygar, E.B.; Gokçeoglu, C. Analytical solutions and 3D numerical analyses of shallow tunnel excavated in weak ground: A case from Turkey. *Int. J. Geo-Eng.* **2021**, *12*, 9. [\[CrossRef\]](#)
38. Aygar, E.B.; Gokceoglu, C. A special support design for a large-span tunnel crossing an active fault (T9 tunnel, Ankara-Sivas high speed railway project, Turkey. *Environ. Earth Sci.* **2021**, *80*, 37. [\[CrossRef\]](#)
39. Geoconsult ZT GmbH. Anatolian motorway stretch-2 bolu tunnels review of geotechnical conditions at Bolu Tunnels. In *Report No: 45.110/R/2125 Revision-1*; Geoconsult: Bolu, Turkey, 1997.
40. Dalgic, S. Tunneling in squeezing rock, the Bolu tunnel, Anatolian Motorway, Turkey. *Eng. Geol.* **2002**, *67*, 73–96. [\[CrossRef\]](#)
41. Dalgic, S. Engineering Geology of the Passage of the Anatolian Motorway through the Bolu Mountains. Ph.D. Thesis, Istanbul University, Istanbul, Turkey, 1994.
42. Geoconsult ZT GmbH. Bolu tunnel geological longitudinal profile a long left tube as built conditions, Asarsuyu portal to Elmalik portal. In *Technical Drawing No. S-050*; Geoconsult: Bolu, Turkey, 1998.
43. O'Rourke, T.D.; Goh, S.H.; Menkiti, C.O.; Mair, R.J. Highway Tunnel Performance during the 1999 Duzce Earthquake. In *Proceedings of the Fifteenth International Conference on Soil Mechanics and Geotechnical Engineering (XV ICSMGE)*, Istanbul, Turkey, 27–31 August 2001.
44. Arioglu, E.; Yilmaz, A.O. *Çözümlü Problemlerle Tünel/Galerilerin Sismik Analizi*; TMMOB Maden Mühendisliği: İstanbul, Turkey, 2006. (In Turkish)
45. Aygar, E.B. Investigation of the Bolu Tunnel Stability by Means of Static and Dynamic Analyses. Ph.D. Thesis, Hacettepe University, Ankara, Turkey, 2007.
46. Aygar, E.B. Evaluation of new austrian tunnelling method applied to bolu tunnel's weak rocks. *J. Rock Mech. Geotech. Eng.* **2020**, *12*, 541–556. [\[CrossRef\]](#)
47. Österreichisches Normungsinstitut. ONORM B 2203. (Österreichisches Normungsinstitut), *Untertagebauarbeiten—Werkvertrag-Snorm*; Österreichisches Normungsinstitut: Vienna, Austria, 1994.
48. Aygar, E.B. A Critical Approach to the New Austrian Tunneling Method in Bolu Tunnels. Master's Thesis, Hacettepe University, Ankara, Turkey, 2000.
49. Geoconsult ZT GmbH. Anatolian motorway stretch 2-bolu tunnels option 3-bernold lining initial support. In *Technical Drawing No. 45.110/R/9464*; Geoconsult: Bolu, Turkey, 1999.
50. Geoconsult ZT GmbH. *Anatolian Motorway Stretch 2 Bolu Tunnels Option 4 Initial Support Section with Deformation Elements*; Technical Drawing No. 45.110/R/9432A; Geoconsult: Bolu, Turkey, 1999.
51. Astaldi, S.p.A. *Geotechnical Measurements Results*; Geodata: Leoben, Austria, 1998.
52. Astaldi, S.p.A. *Geotechnical Measurements Results*; Geodata: Leoben, Austria, 1996.
53. Hoek, E.; Marinos, P. Predicting tunnel squeezing. In *Tunnels and Tunnelling International. Part 1—November 2000, Part 2—December 2000*; 2000. Available online: <https://www.rocsience.com/assets/resources/learning/hoek/Predicting-Tunnel-Squeezing-Problems-in-Weak-Heterogeneous-Rock-Masses-2000.pdf> (accessed on 13 October 2023).
54. Jethwa, J.L.; Singh, B. Estimation of Ultimate Rock Pressure for Tunnelings under Squeezing Rock Conditions. A New Approach. In *Proceedings of the ISRM Symposium, Design and Performance of Underground Excavation*, Cambridge, UK, 3–6 September 1984.
55. Hoek, E.; Brown, E.T. *Underground Excavations in Rock*; Instn Min. Metall: London, UK, 1980.

56. Hoek, E. Rock Support Interaction Analysis for Tunnels in Weak Rock Masses. 2012. Available online: <https://www.rocscience.com/documents/pdfs/rocnews/winter2012/Rock-Support-Interaction-Analysis-for-Tunnels-Hoek.pdf> (accessed on 4 November 2022).
57. Vlachopoulos, N.; Diederichs, M.S. Improved longitudinal displacement profiles for convergence confinement analysis of deep tunnels. *Rock Mech. Rock Eng.* **2009**, *42*, 131–146. [[CrossRef](#)]
58. Brady, B.H.G.; Brown, E.T. *Rock Mechanics for Underground Mining*; Allen and Unwin: London, UK, 1985.
59. Durukal, E. Critical evaluation of strong motion in Kocaeli and Düzce (Turkey) Earthquakes. *Soil Dyn. Earthquake Eng.* **2002**, *22*, 589–609. [[CrossRef](#)]
60. Menkiti, C.O.; Mair, R.J.; Miles, R. Tunneling in complex ground conditions in Bolu. In Proceedings of the Underground Construction, London, UK, 18–20 September 2001.
61. Kaptan, K.; Tezcan, S. Deprem dalgalarının zemin büyütmesi üzerine örnekler. *Turk. Sci. Res. Found.* **2012**, *5*, 17–32. (In Turkish)
62. Geoconsult ZT GmbH. *Anatolian Motorway Gümüşova-Gerede Section 2 Bolu Tunnel, Collapse in Bolu Tunnel (Elmalik Side) Interim Report*; Report No: 45.110/R/2170; Geoconsult ZT GmbH: Bolu, Turkey, 2000.
63. Geoconsult ZT GmbH. *Anatolian Motorway Gümüşova-Gerede Section 2 Bolu Tunnel, Elmalik Left Tube Comparative Longitudinal Section*; Drawing No: 45.110/15513; Geoconsult ZT GmbH: Bolu, Turkey, 2000.
64. Lombardi Eng. Ltd. *Gümüşova-Gerede Motorway Asarsuyu Tunnels, Detailed Seismic Analysis-op.3 op.4 and Active Fault Crossing-Design Philosophy and Joint Requirements*; Astaldi: Bolu, Turkey, 2001.
65. Isik, S.; Ozben, M. Assessment of deformation effects of 12 November 1999 Düzce earthquake on Bolu tunnels and seismic design. In Proceedings of the Sixth National Conference on Earthquake Engineering, Istanbul, Turkey, 16–20 October 2007; pp. 709–722.
66. Astaldi, S.p.A. *Geotechnical Measurements Results*; Geodata: Leoben, Austria, 2003.
67. Russo, M.; Germani, G.; Amberg, W. Tunnel through active faults: A recent application. In Proceedings of the International Conference of Tunnelling & Underground Space Use, Istanbul, Turkey, 16–18 October 2002.

Disclaimer/Publisher's Note: The statements, opinions and data contained in all publications are solely those of the individual author(s) and contributor(s) and not of MDPI and/or the editor(s). MDPI and/or the editor(s) disclaim responsibility for any injury to people or property resulting from any ideas, methods, instructions or products referred to in the content.